CONTRIBUTED PAPER

Wide Bandgap DC–DC Converter Topologies for Power Applications

This article reviews new WBG architectures and new WBG semiconductor technologies, with respect to their application in the field of power electronics.

By Mohammad Parvez, Aaron T. Pereira, *Member IEEE*, Nesimi Ertugrul, *Senior Member IEEE*, Neil H. E. Weste, *Life Fellow IEEE*, Derek Abbott, *Fellow IEEE*, and Said F. Al-Sarawi, *Member IEEE*

ABSTRACT | Over the last decade, dc–dc power converters have attracted significant attention due to their increased use in a number of applications from aerospace to renewable energy. The interest in wide bandgap (WBG) power semiconductor devices stems from outstanding features of WBG materials, power device operation at higher temperatures, larger breakdown voltages, and the ability to sustain larger switching transients than silicon (Si) devices. As a result, recent progress and development of converter topologies, based on WBG power devices, are well-established for power conversion applications in which classical Si-based power devices show limited operation. Currently, Si carbide (SiC) and gallium nitride (GaN) are the most promising semiconductor materials that are being considered for the new generation of power devices. The use of new power semiconductor devices, such as GaN high electron mobility transistors (GaN HEMTs), leads to minimization of switching losses, allowing high switching frequencies (from kHz to MHz) for realizing compact power converters. Finally, design recommendations and future research trends are also presented.

KEYWORDS | DC–DC converter; gallium nitride (GaN); high electron mobility transistors (HEMTs); MOSFETs; power devices; silicon carbide (SiC); wide bandgap (WBG) semiconductors.

Manuscript received September 19, 2020; revised February 11, 2021; accepted April 2, 2021. Date of publication April 29, 2021; date of current version June 22, 2021. *(Corresponding author: Derek Abbott.)*

The authors are with the School of Electrical and Electronic Engineering, The University of Adelaide, Adelaide, SA 5005, Australia (e-mail: derek.abbott@adelaide.edu.au).

Digital Object Identifier 10.1109/JPROC.2021.3072170

I. INTRODUCTION

A key objective in power converter design is to decrease power losses to improve the conversion efficiency—this impacts applications such as in renewable energy. By decreasing the power loss, the size of the converter components can be reduced, which leads to a compact size for the whole converter [1], [2].

Therefore, the converter size and cost fully depend on the design requirements and applications, where the power density of the converter is inversely proportional to the size of its passive components. Due to the increased switching frequency, the power density and switching loss increase, resulting in decreasing converter efficiency. Moreover, these switching losses can be reduced by using several soft switching (SS) techniques, which increases the complexity of the converter circuit.

In the last decade, crucial research has focused on isolated dc–dc converters to improve the conversion efficiency and voltage gain, as well as reducing the switching losses [1], [3]–[7]. The majority of power converters can be unidirectional to deliver power to loads, such as motor drives, uninterruptable power supplies, renewable energy sources, and battery chargers. On the other hand, in other applications, it becomes a requirement to have converters with bidirectional power conversion properties—a good example of this is in renewable energy combined with battery storage applications. A possible way to consider the classification of WBG power dc–dc converter topologies is in terms of integrated converters and discrete power converters. In contrast to discrete converters, where the interest is in high efficiency, integrated converters focus on integrating the underlying logic functions in such control

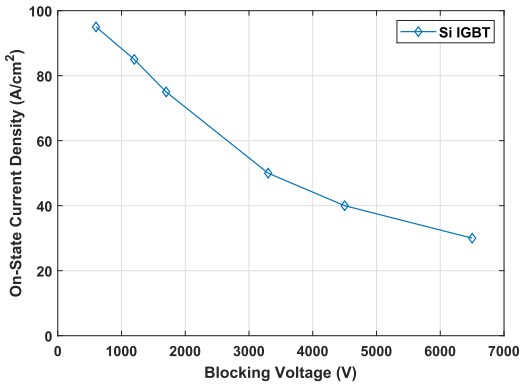

Fig. 1. *ON-state characteristics currve of IGBT devices [17].*

circuits on the same die to result in a highly integrated, power-efficient, reduced system complexity, low cost, and small area—for a wide range of applications, such as electric vehicles (EVs), switched-mode power supplies, and dc motor drivers. Historically, silicon (Si) MOSFET technology is well-established in power semiconductor devices [8]. Recently, WBG semiconductor materials have been introduced in the power semiconductor market. Among the various WBG devices, Si–carbide (SiC) and gallium–nitride (GaN) devices deliver superior power converter performance due to their outstanding material features in comparison to Si devices [9]–[11]. Extensive studies have been performed on well-recognized SiC power devices [12], [13]. On the other hand, there are only a few studies on GaN devices for high-power (HP) applications (up to a few kW) [14], [15].

This article reviews new WBG architectures and new WBG semiconductor technologies, with respect to their application in the field of power electronics. High-frequency (HF), high-efficiency, switched-mode power converter circuits using GaN on Si-based integrated circuits are suitable for downstream applications, including automotive and renewable energy technologies.

Today's Si power MOSFET and Si insulated-gate bipolar transistor (IGBT) are the main building blocks of power electronics switching circuits [16]. Advanced Si IGBTs with blocking voltage capability ranging from 600 to 6500 V are emerging due to the large variety of high-volume applications [17]. In the last five years, SiC devices have become commercially available with the potential to replace Si IGBTs in a number of applications. However, penetration into the IGBT market is still constrained by the high manufacturing cost of SiC devices. The ON-state characteristic curve of IGBT devices is shown in Fig. 1 as a function of blocking voltage capability. It can be seen from the figure that the reduction in the ON-state current density for IGBTs results in an increase in the blocking voltage. The ON-state current density is determined by thermal consideration, such as the maximum junction temperature of the package [18]. However, Si power semiconductor devices suffer from several issues [19].

1) *High losses:* The relatively low Si bandgap (1.1 eV) and low critical electric field (30 V/μm) result in high-voltage devices with substantial thickness, leading to higher conduction losses.
2) *Low switching frequency:* Si power MOSFETs incur high conduction losses due to majority carriers and hard switching operation. The gate charge capacitance produces a high spike current, which leads to increased conduction losses and switching losses at high switching frequencies. On the other hand, Si IGBTs have higher current density compared to Si MOSFETs due to minority carriers and conductivity modulation. The minority carriers reduce the switching frequency range of IGBTs, resulting in low switching losses. Low switching frequency also leads to larger inductors and capacitors, resulting in bulkier systems.
3) *High leakage current and high temperature:* Typically, the junction temperature and leakage current depend on the high intrinsic carrier density, resulting in the high intrinsic carrier density of Si power devices leading to an increase in the junction temperature and the leakage current. The maximum operating junction temperature of IGBTs is typically 125 °C.

In the recent development of power semiconductor devices, several researchers have tried to alleviate these problems by using WBG semiconductors. These WBG-based converters are able to obtain high efficiency and high voltage gain due to low switching losses, at high operating voltages (>1 kV to tens of kV), high operating frequencies (tens of kHz to tens of GHz), and high operating temperature (>150 °C) [20]–[22]. Hence, GaN on Si delivers superior performance to bulk Si technologies while being more cost-effective than GaN on SiC, GaN on GaN, or GaN on diamond [23].

Typically, dc–dc converters are classified into isolated and nonisolated converters, as shown in Fig. 2. The isolation refers to the electrical barrier between the inputs and outputs of the converter. An HF transformer can be used as an electrical barrier in the converter. The benefits of the barrier are in facilitating high-voltage applications with different output voltage polarities [24]. Several converter topologies and applications are proposed to increase the efficiency of isolated dc–dc converters [6], [7], [23]. Most isolated dc–dc converters utilize zero voltage switching (ZVS) to improve the efficiency up to 97% for HP converters ranging from 1 to 5 kW [25], [26]. However, it is quite challenging to further improve the efficiency of nonisolated converters.

In contrast to Si technology, GaN is a promising semiconductor for HP converters for further improving switching losses resulting in increased efficiency [10]. There are still some limitations in the manufacturability of GaN devices, and the cost of GaN devices is higher than Si. Recently, manufacturers have been continually addressing these limitations, reducing GaN development cost aiming for GaN devices with cost equivalence to Si [10]. Another limitation of WBG devices is the packaging due to the parasitic inductances in the device and printed circuit board (PCB)

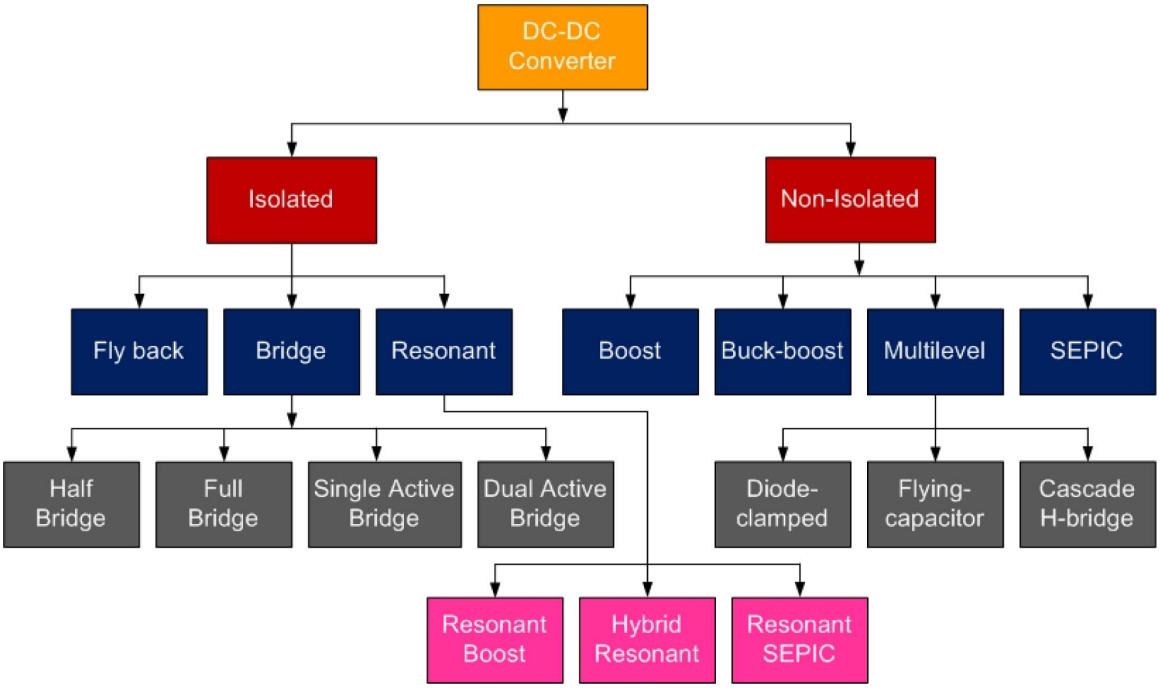

Fig. 2. *Classification of dc–dc converters.*

traces [27]. These devices are more popular due to low switching loss and frequency operation but with high junction temperature [10]. To enable miniaturization and full utilization of the GaN devices, HF operation is needed, so parasitics associated with on-chip interconnects and loads must be minimized. For loads, such reduction can be achieved either using the point-of-load (PoL) approach or utilizing an integrated voltage-regulator (IVR) [28], [29].

This article is organized into five sections. Section II presents and describes classical power dc–dc converter topologies. Then, in Section III, recent progress and development in wide bandgap (WBG) power devices and major challenges are described. In Section IV, WBG-based power dc–dc converter topologies are presented, where we have only focused on low- to mid-power WBG dc–dc converter topologies for comparison and classification with the proposed converter topology, while we have proposed a low-power dc–dc converter with low input dc voltage applied to obtain high output voltage gain and high efficiency. These converter topologies available in the literature are capable of offering either high voltage gain or can handle power levels within 180–2400 W, as will be shown later in Table 17. Design recommendations, followed by future research trends are discussed in Section V.

II. CLASSICAL POWER DC–DC CONVERTER TOPOLOGIES

To understand the recent development and implementations of WBG power dc–dc converter topologies, it is important to first provide a brief summary of classical Si-based power devices and their applications in the last decade. In the 1970s, thyristor-based dc–dc buck-boost (BB) converters were established for HP applications [30]. A a few years later, a multilevel converter (MC) was proposed [31], controlled by using a time-sharing HF to provide large-scale dc power supplies, which can operate over an ultrasonic chopping frequency with frequencies above 20 kHz.

In the last three decades, MCs have been designed and developed for medium-power (MP) to HP applications [32]–[37]. These converters featured both HF and SS techniques combined with a three-phase symmetric ac link transformer. Generally, these converter topologies (such as resonant converters and bridge/multiphase bridge converters) may be considered as classical dc–dc converter topologies and are used in several power applications.

A. Classical Silicon-Based Power Devices

Si-based power devices can be classified into buck converters, resonant boost converters, resonant converters, and resonant single-ended primary-inductor converters (SEPICs). Several traditional circuit configurations are described based on the MOSFET/IGBT. Although, both IGBT and MOSFET are voltage-controlled semiconductor

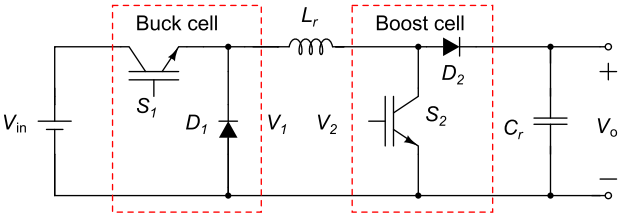

Fig. 3. *TSBB converter.*

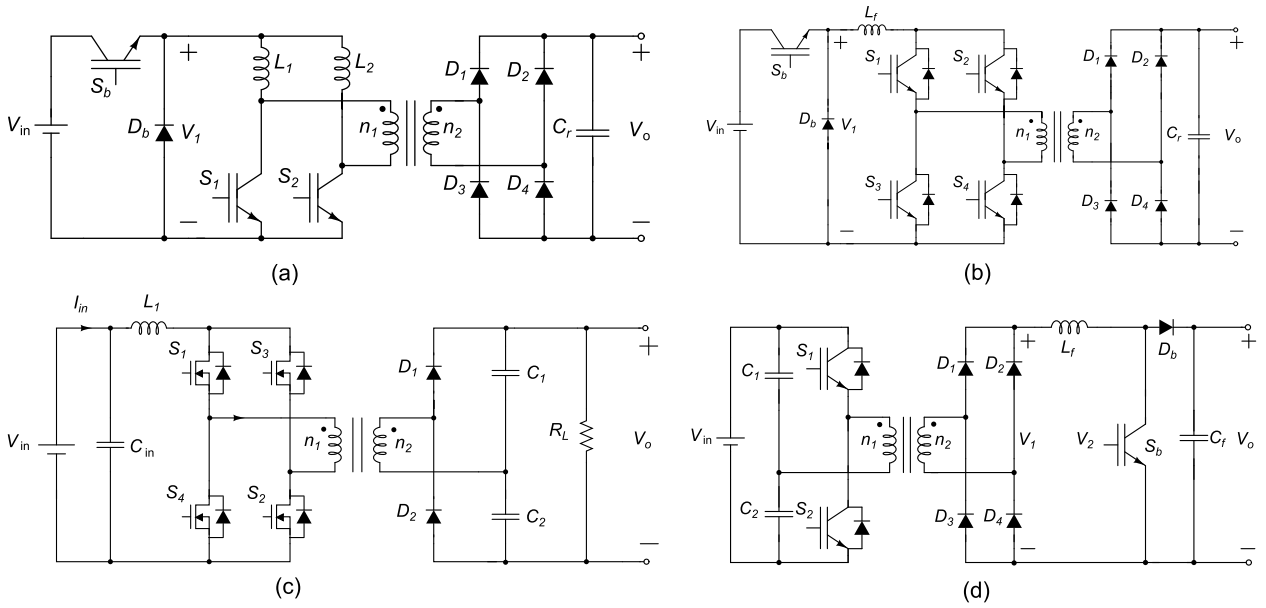

Fig. 4. ***Isolated BB converter [39], [43] with (a) HB buck converter, (b) FB buck converter, (c) FB-boost converter, and (d) HB-boost converter.***

devices that operate well in switched-mode power supply (SMPS) applications, IGBTs possess improved power handling capability [38]. The IGBT has a lower forward voltage drop compared to the MOSFET. With the increase in selections between the two devices, it is becoming more problematic to select the best device based on their applications alone. Typically, MOSFETs operate at higher switching frequencies around 200 kHz, where IGBTs operate at low switching frequencies around 10–20 kHz. The two-switch BB (TSBB) converter, as shown in Fig. 3 [39], is constructed by using buck and boost cells' combination.

A well-known classical HF isolated buck dc–dc converter can be obtained, as shown in Fig. 4(a) and (b), by substituting the buck cell in Fig. 3. Similarly, the isolated boost converter can be constructed, as shown in Fig. 4(c) and (d), by substituting the boost cell in Fig. 3. Moreover, a resonant tank circuit can be described as the boost converter, the BB converter, the SEPIC converter, or the hybrid bridge converter to obtain SS resonance. The voltage across the switching elements may be made by putting one or more components of the LC network in series or parallel with the converter switches, so they can turn on–off with ZVS [40]–[42]. In addition to the zero switching voltage and current of the active switches, this topology also has a zero switching current for the output diodes.

Nevertheless, normally, the switching frequency has to be higher than the preferred resonance frequency in order to guarantee SS operation and to obtain output voltage or current over a wide range. This tends to result in a bulky resonant tank, low power density, and poor efficiency. An example of various types of resonant converter topologies is shown in Fig. 5(a)–(c). Traditionally, dc–dc resonant converters are built for low-frequency and

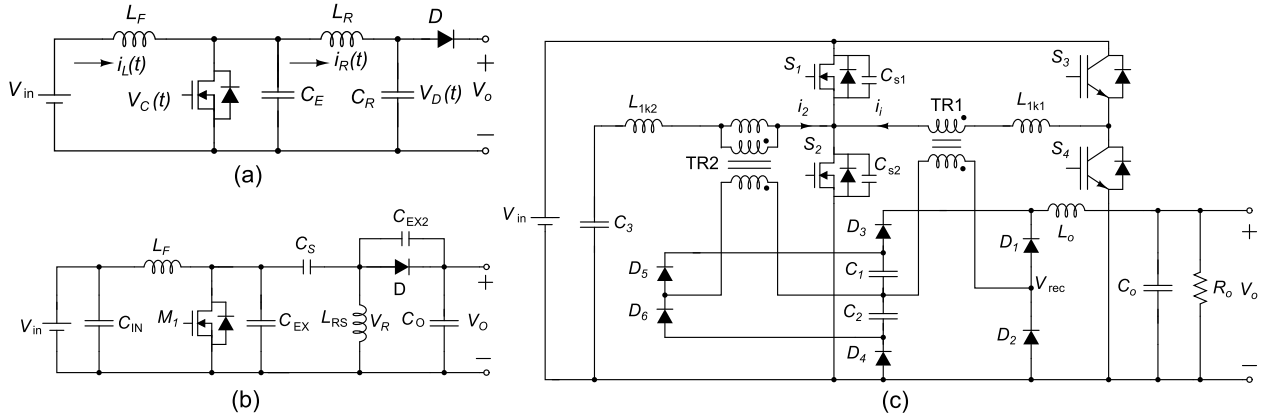

Fig. 5. ***(a) Resonant boost converter [44]. (b) Hybrid resonant and phase shift converter [7]. (c) Resonant SEPIC converter [45].***

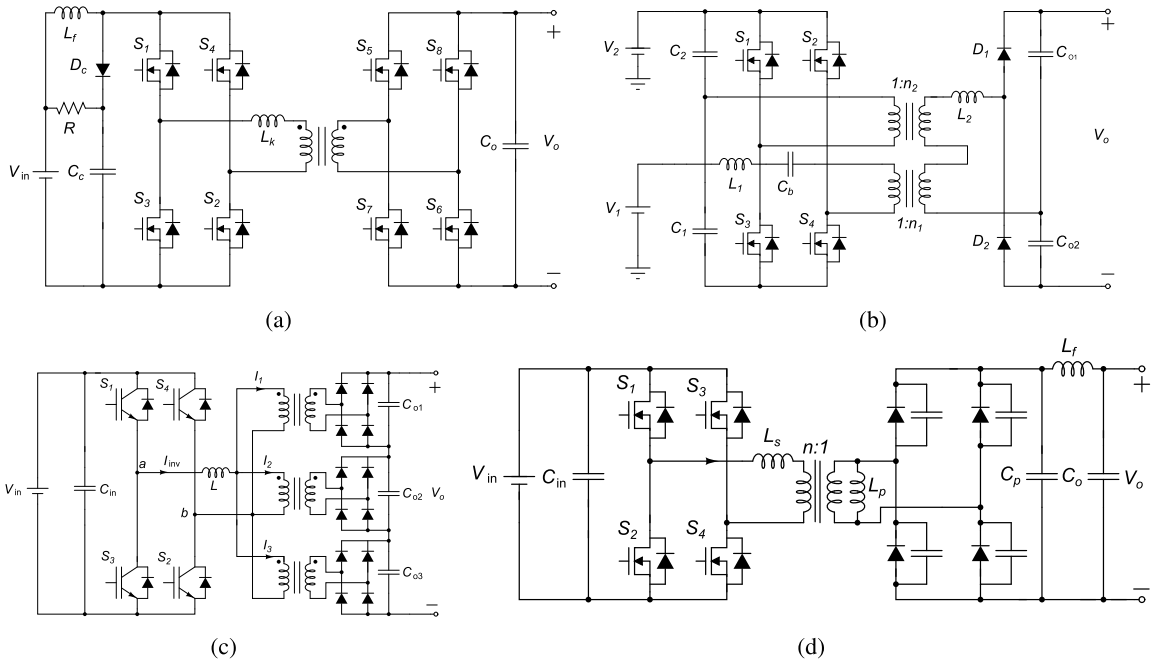

Fig. 6. *(a) Bidirectional isolated FB-boost converter [39], [46]. (b) HB-boost and FB converter [39], [47]. (c) HV dc–dc FB converter [39], [48]. (d) SPCD converter topology [39], [49].*

low-power applications, such as telecommunications, fuel cell-based power systems, and renewable power supplies. These topologies are limited by the use of semiconductor device switches. To overcome these problems, recently, several types of HF or very HF (VHF) resonant converters were built for medium-output-power applications [4], [7], [40]–[42].

Moreover, bridge dc–dc power converters have been significantly developed and implemented in recent years [46]–[49]. Fig. 6(a)–(d) shows existing implementation of isolated full bridge (FB) converter topologies for HP applications. Due to SS techniques, such as ZVS or zero current switching (ZCS) techniques, a possible decrease in system switching losses and an improvement in switching frequency are possible. In the same way, an SS pulsewidth modulated (SS-PWM) FB bidirectional isolated converter is constructed for step-up function, as shown in Fig. 6(a), where its communication process is developed to reduce the mismatch between the leakage inductor and boost inductor current when communication occurs.

In [47], the dual-input-based dc–dc converter is reported where it consists of an HB-boost cell and FB-boost cell combination, as shown in Fig. 6(b). Though this strategy has some benefits, the major problem is the current stress that raises the design complexity. In addition, due to the dead-time effect, where a capacitor charging-based high-voltage (HV) dc–dc converter is implemented for HP application, as shown in Fig. 6(c) [48], it contains an FB converter and three HV-HF transformers. A series–parallel current-driven (SPCD)-based FB converter is represented in Fig. 6(d) [49], while these branch combinations L_s, L_p, and C_p offer ZVS to improve the converter efficiency [50].

B. Multilevel Converter

The classical and recent advances in MCs can be divided into three groups: the capacitor clamp (CC) converter or the diode-clamped (DiC) converter, the cascade H-bridge (CHB) converter, and the flying capacitor (F-C) converter [51]–[53]. These MCs can be used to obtain higher operating voltage and reduce the voltage stress across switches. Note that dc–dc MCs with a transitional ac link are based on the well-known dc–ac MC. In this section, the modular MC (MMC) is also addressed.

Recently, three-level (3L) dc–dc converter topologies with an LLC resonant circuit have been proposed in HP and MP applications, as shown in Fig. 7 [54], where the neutral point clamping (NPC) structure is used by neglecting NPC diodes [54]. The LLC resonant circuit is presented to obtain the SS operation, which provides a stable dc output voltage. A three-phase 3L dc–dc converter

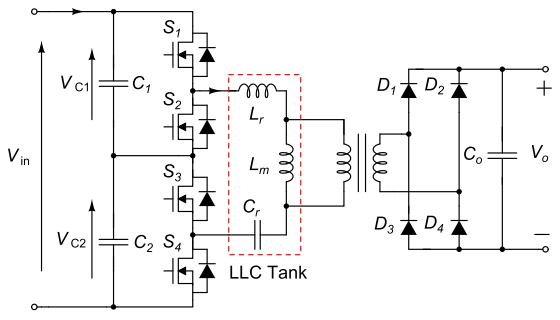

Fig. 7. *3L dc–dc converter with the LLC resonant tank [39], [54].*

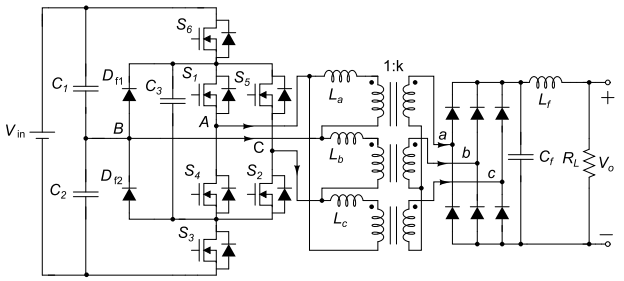

Fig. 8. ***Three-phase 3L dc–dc converter [39], [55].***

is shown in Fig. 8. This converter topology is a combination of an FB converter and a 3L HB converter that uses a symmetrical duty cycle to control the high-input-voltage and HP applications [55]. Therefore, the switching devices decrease to half of the input voltage upon each voltage stress, and the output current ripple frequency sufficiently improves. This can be adopted to minimize the filtering requirement. Increasing the switching losses decreases the overall performance of the converter due to a hard switching method; therefore, the SS (ZVS/ZCS) strategy may address this limitation. Fig. 9 shows the bidirectional dc–dc converter with a hybrid switching circuit [56]. Moreover, several types of DiC converter and NPC-based MC topologies have been studied [56], [57]. The significant research interest also shows on F-C-based dc–dc converter topologies in the literature [58], [59].

Fig. 10 shows a four-level (4L) F-C-based bidirectional nonisolated dc–dc converter that contains six switching operating cells creating three switching poles [59]. Note that the converter (see Fig. 10) does not use any magnetic components with a PWM technique to produce a fixed duty cycle. Furthermore, the structure is usually used as a voltage multiplier [59]. Therefore, these types of topologies have some limitations, such as complexity, high switching frequency, overvoltage drop, nonmodular layout, complicated switching methods, and bidirectional power flow limitation.

Currently, the multilevel cascade dc–dc converter is gaining increased interest in photovoltaic (PV) applications [60]–[64]. Such a topology can be designed using either a buck or boost converter for PV applications.

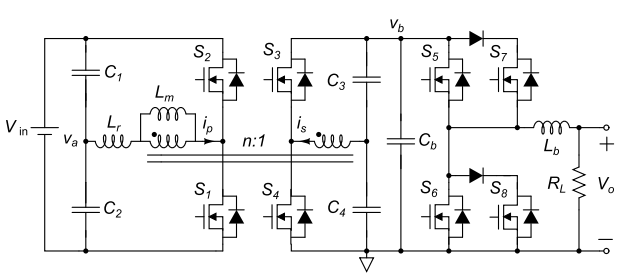

Fig. 9. ***Two-stage isolated bidirectional dc–dc converter [39], [56].***

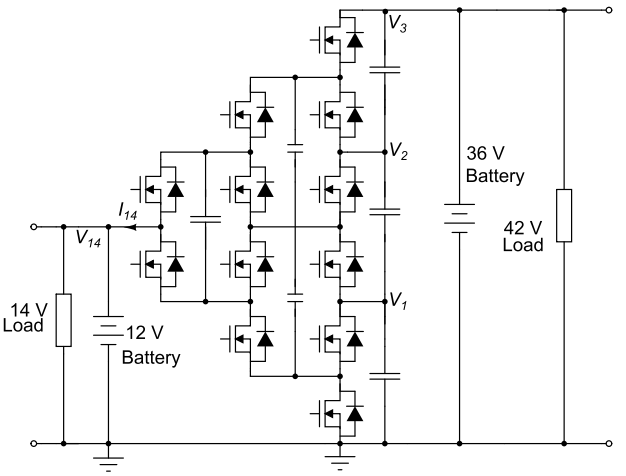

Fig. 10. ***Multilevel (4 L) F-C-based bidirectional nonisolated dc–dc converter [39], [59].***

A comparison between the three multilevel topologies is given in Table 2 [51], [58]–[64]. As an example, a buck-type multilevel cascade dc–dc converter topology proposed for PV applications is shown in Fig. 11 [60]. The freewheeling diode in this converter allows current bypassing in case of PV module failure. On the other hand, some active device components can have continuous operation during a fault condition. Performance comparison of Si-based converter topologies is shown in Table 1 [30], [39], [65]–[76]. From the table, it can be seen that the bridge/multiphase converter is capable of delivering both HP with high output voltage in comparison to resonant and MCs although the resonant converter has the advantage that it can operate at high switching frequency. Note that bridge, multiphase, and MCs can be based on BJT, MOSFET, or IGBT devices, whereas resonant converters use both SCR and MOSFET devices. Modulation control

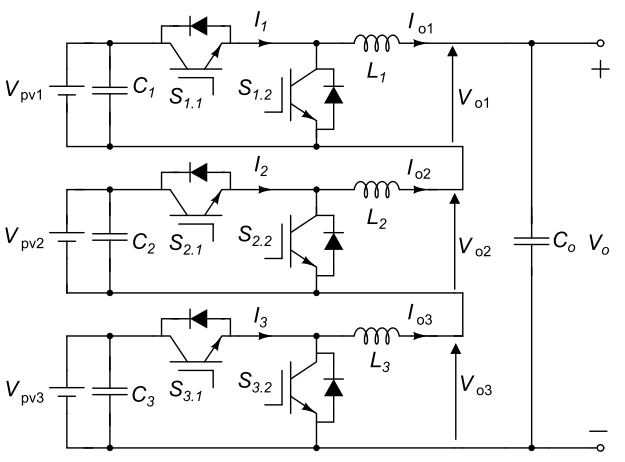

Fig. 11. ***Multilevel cascaded dc–dc HB converter topology for PV applications [39], [60].***

Table 1 Performance Comparison of Si-Based Several Power DC–DC Converter Topologies [39]

Parameters	Resonant Converter	Multilevel Converter	Bridge/Multiphase Converter
Power rating (kW)	2.74, 5, 24, 50	2.75, 3, 12.6	2, 2.8, 3, 6, 40, 50
Output voltage (V)	400, 600	43, 700	60, 220, 280, 300, 350, 400,600, 2000
Switching frequency (kHz)	100, 120, 250, 750	33.3	10, 20, 25, 50, 100, 200, 256
Semiconductor devices	SCR, MOSFET	MOSFET	BJT, MOSFET, IGBT
Modulation and control techniques	PWM	PWM, PS-PWM	PWM, PS-PWM, DPS-PWM
Control variable	Voltage control	Voltage Control/Current Control	Voltage Control/Current Control
Switching loss	High	Comparatively low	Low
Converter efficiency	Low	Comparatively high	High
References	[30], [65], [66], [67], [68].	[69], [70].	[71], [72], [73], [74], [75], [76].

techniques, such as PWM, PS-PWM, and DPS-PWM can be used in the bridge/MC, whereas both resonant and MCs are limited to PWM and PS-PWM modulation and control techniques.

As can be noted from Table 2, a cascade half-bridge (CHB) MC is favorable for PV applications compared to DiC- and F-C-based MCs because it uses fewer switches and has lower voltage stress, easier switching signal control, fault-tolerance capability, lower harmonic distortion for higher switching frequencies, reduced circuit complexity, low cost, and smaller size.

III. RECENT PROGRESS AND DEVELOPMENT IN WIDE BANDGAP POWER DEVICES

New development of high-efficiency power converters has emerged with the advancement of WBG power semiconductor materials [1]. In a majority of power converters, magnetic components (inductors and transformers) and capacitors contribute significantly to the overall converter size and cost. Therefore, to miniaturize and reduce the cost of an electrical energy processor, its switching frequency, f_{SW}, must be increased [16]. Emerging low-loss circuit components are required for HP applications. This is the basic reason for promising WBG power devices; they also lead to increased energy efficiency in traditional Si-based power converters and open new HV HP conversion applications. Fig. 12 shows an ON-state characteristic curve of a WBG power device compared to an Si IGBT power device as a function of blocking voltage rating. It may be noted from the figure that the current density reduces for both Si IGBT and SiC MOSFET devices when increasing the blocking voltage rating.

In the last few years, a large number of HF, high-efficiency, integrated power electronics based on WBG devices using GaAs, SiC, and GaN technologies have been reported; some converters are combined with Si or GaAs-based logic circuits for control. The underlying logic functions in such control circuits can be integrated on the same die as the converter to develop highly integrated, power-efficient, and small-area modules for a wide range of applications, such as EVs, switched-mode power supplies, and dc motor drivers. Such an approach results in superior performance compared to existing GaN modules interfaced with Si- or GaAs-based technologies while maintaining low cost [1]. Fig. 13 shows the performance of both GaN and SiC technologies in comparison with Si-based and demonstrates that GaN performance exceeds other technologies in all aspects except for thermal conductivity, which is improved in the case of SiC technology [77].

A. SiC-Devices

It may be noted that SiC power devices are the most developed WBG semiconductors. These devices have progressed significantly since 1987 due to CREE Inc., which

Table 2 Performance Comparisons of Si-Based Three MC Topologies [51], [58]–[64]

Parameters	Diode-clamped (DiC)	Flying-capacitor (F-C)	Cascaded H-bridge (CHB)
Discharge	Less	Higher	Higher
Filter components	Reasonable	Bulk	Light
Modular structure	No	No	Yes
Voltage stress	N/A	Higher	Lower
Fault tolerance	N/A	Unable	Capable
Necessity of switching devices	Higher	Less	Lower
Switching system	N/A	Difficult	Easier
Gate signal	N/A	N-phase signal	Two-phase signal
Voltage drop on active devices	Reasonable	Higher	Lower
Capacitors used	N/A	Higher and different values	Lower and same values

Table 3 Comparison Figure of Merit for WBG Semiconductor Materials With Respect to Si [80], [81]

Figure-of-merit name	Si	6H-SiC	4H-SiC	GaN
Johnson's figure of merit (JFM)	1.0	277.8	215.1	215.1
Baliga's figure of merit (BFM)	1.0	125.3	223.1	186.7
FET switching speed figure of merit (FSFM)	1.0	30.5	61.2	65.0
Bipolar switching speed figure of merit (BSFM)	1.0	13.1	12.9	52.5
FET power-handling-capacity figure of merit (FPFM)	1.0	48.3	56.0	30.4
FET power switching product (FTFM)	1.0	1470.5	3424.8	1973.6
Bipolar power handling capacity figure of merit (BPFM)	1.0	57.3	35.4	10.7
Bipolar power switching product (BTFM)	1.0	748.9	458.1	560.5

is the main provider of SiC wafers. Note that SiC Schottky diodes have higher blocking voltage capability compared to Si Schottky diodes. Apart from commercial devices, many other SiC devices are operated in the kV range with minimized ON-resistances using 4H-SiC and 6H-SiC p-n diodes, Schottky diodes, IGBTs, thyristors, BJTs, several MOSFETS, or gate turn-off thyristors (GTOs). Therefore, with some exceptions, the specified devices have very low current ratings.

The use of SiC power devices can improve system-level gains, such as minimization of switching losses, size, volume, and increased efficiency. When SiC power devices are implemented in a hybrid EV (HEV) instead of Si power devices, the efficiency increases by 10%, and the heatsink is reduced to 1/3 of the original size [78], [79]. Currently, two SiC polytypes, such as 6H-SiC and 4H-SiC, are well-studied in the research domain, but 4H-SiC is presently more dominant for applications. Although both of these polytypes possess similar properties, 4H-SiC is more popular over 6H-SiC because the carrier mobilities in 6H-SiC are not identical in the vertical and horizontal directions, whereas the carrier mobilities in 4H-SiC are identical in orthogonal directions [80].

Furthermore, a performance comparison of promising power electronics technologies, using well-known figures of merit, normalized relative to Si-based transistors, is shown in Table 3 [80], [81]. As can be seen, Si transistors present the poorest performance among the semiconductor materials, whereas SiC and GaN have almost the same figures of merit, except when it comes to thermal conductivity for SiC technology [77]. Hence, current research activities are directed toward creating GaN on different substrates to improve the thermal conductivity performance [82], [83].

Recently, Infineon has released their CoolSiC generation 6 (G6) for SiC Schottky barrier diodes with a breakdown voltage of 650 V (Infineon-IDH04G65C6, PG-T0220-2 data sheet). This represents an enhancement over the CoolSiC G5 via advancements, such as a novel Schottky metal system. The implementation of highly efficient, compact, and simple three-phase inverter systems is currently limited by high dynamic losses operating at 1200 V in Si devices. Alternative designs using 600-V/650-V devices can result in partially improved efficiency. However, such designs result in higher cost and module complexity when integrated into multilevel topologies, resulting in more complex control systems. In addition, Infineon TRENCHSTOP technology has provided HP IGBT modules from 1200 to 3300 V with a current rating ranging from 200 to 1500 A, especially for motor control drives, wind energy systems, solar energy systems, uninterruptible power supply (UPS), and agricultural vehicles, which means much lower static losses, higher power density, and softer switching [84].

Furthermore, Littelfuse, Wolfspeed, and Microsemi provide advanced SiC devices that use Schottky barrier diodes with high breakdown voltage in the order of 1700 V, while

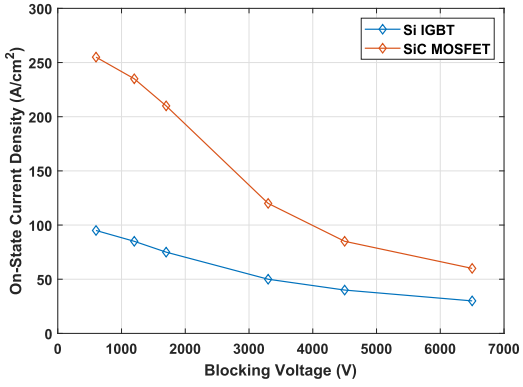

Fig. 12. *ON-state characteristics curve of WBG power device is compared with Si IGBT [17].*

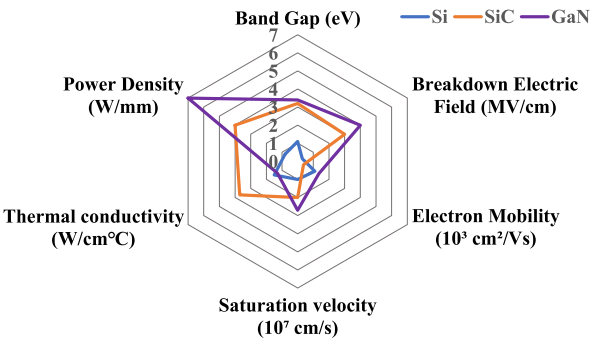

Fig. 13. *Summary of material properties for Si, SiC, and GaN [77].*

Table 4 Static Characteristics of SiC MOSFETs for Infineon's IDH04G65C6, Littlefuse's 1700-V N-Channel LSIC1MO170E1000, the 3330-V GR350MT33J, and Infineon's IGBT4 for the FZ2000R33HE4-IGBT4 Module That Are Commercially Available

Parameters	SiC MOSFET Infineon (IDH04G65C6)	SiC MOSFET Littelfuse (LSIC1MO170E1000 1700 V)	SiC MOSFET GenSiC (GR350MT33J-3300 V)	IGBT4 Infineon (FZ2000R33HE4 IGBT4)
Drain-source voltage (V_{DS})	650 V	1700 V	3300 V	3300 V
Drain current (I_{D})	4 A	3.5 A	400 A	2000 A
Drain-source on-resistance, $R_{\mathrm{DS(on)}}$	0.315 Ω	750 mΩ	350 mΩ	N/A
Maximum junction temperature (T_j)	150°C	150°C	150°C	150°C

GeneSiC has a newly developed 3300-V, 400-A SiC power module. The static characteristics of the SiC MOSFET for Infineon's IDH04G65C6, Littlefuse's 1700-V N-channel LSIC1MO170E1000, the 3330-V GR350MT33J, and Infineon's IGBT4 for the FZ2000R33HE4-IGBT4 module are shown in Table 4.

B. GaN-Devices

At the heart of a high-efficiency converter is a low-loss, high-voltage, high-current power switch that can deliver variable output power. The high efficiency within a switching power converter is obtained by the choice of semiconductor technology used, as well as the peripheral drive and control topology of the system. High-quality lateral heterostructures (e.g., AlGaN/GaN) with high electron mobility transistors (HEMTs) and high 2-D electron gas (2DEG) density make GaN an ideal semiconductor of choice for power devices. One of the key benefits of lateral device technology is its high integration density, which can be exploited for the development of on-chip peripheral control circuits [85]. In contrast to Si design methodology developments, which have been in practice for almost 40 years, only the power devices themselves are integrated onto GaN chips. However, to enable low-cost, high-efficiency circuits, there is a need to integrate the control logic circuitry onto the GaN chips. This requires the development of new circuit, logic, and design strategies to deal with this requirement. This arises because, for the last 70 years, the focus has been on Si technology, and billions of dollars have been invested into the development of that technology.

1) GaN Rectifiers: Currently, most GaN Schottky diodes use a lateral configuration to overcome the conduction losses in GaN substrates [86]. Moreover, both the forward and breakdown voltages in lateral GaN rectifiers are still high, where 9.7-kV breakdown voltages have been found on sapphire substrates [82]. Note that GaN rectifiers on Si substrates are more demanding significant attention because of their lower cost. Furthermore, currently, high-junction temperature GaN substrates and 600-V GaN Schottky diodes are commercially available in the market. Recently, a 1500-V lateral GaN Schottky diode structure has been reported [87]. Note that GaN junction barrier Schottky (JBS) diodes can further increase the operating voltage of these rectifiers from 1500- to 3000-V voltage range.

2) High Electron Mobility Transistors and Power MOSFETs: One of the important features of GaN is the presence of a 2DEG shaped in AlGaN/GaN lateral heterostructures due to a large conduction band. The existence polarization fields in AlGaN/GaN can be allowed a large 2DEG concentration with high electron mobility values from 1200 to 2000 cm^2/Vs. Fig. 14 shows a normally-on GaN HEMT, where a negative bias is applied between the gate and the source to modulate the drain-to-source current. Nowadays, these devices are becoming more and more popular due to their HP switching frequency with outstanding performance tradeoff between explicit ON-resistance and breakdown voltage. In addition, these are suitable for high switching applications with ultrahigh bandwidth and as microwave power devices for cellular phone base stations.

Note that GaN-based HEMTs devices have been designed and developed on both sapphire and SiC substrates at HF to demonstrate their output power performance from 1.1 to 40 W/mm [88], [89]. Furthermore, GaN HEMTs are emerging with capability up to 10 kV, while GaN-based converters have already been established. One of the limiting factors affecting GaN-based HEMT configurations is the reduced drain current failure and enhancement of the gate to drain breakdown voltage due to adjusting the size and superficial thicknesses [90]. In this case, various control techniques have been considered with a superficial-charged-controlled n-GaN cap configuration by using Si nitride [91].

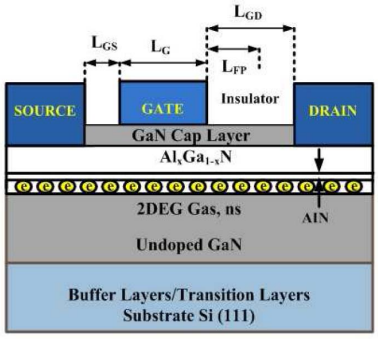

Fig. 14. *Cross section of a typically-on GaN HEMT [9].*

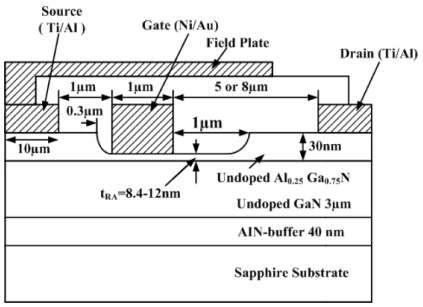

Fig. 15. *Recessed-gate GaN HEMT structure [9], [96].*

Note that the blocking voltages of AlGaN/GaN lateral heterostructures are higher than 1 kV [92] when mounted on Si substrates. Moreover, high blocking voltage capability and low ON-resistance of GaN HEMTs on SiC substrates have been realized, giving rise to a record figure-of-merit ($\sim 2.3 \times 10^9$ $V^2/\Omega \cdot cm^2$) beyond the 6H-SiC theoretical limit [93]. Recently, a 2.2-kV GaN HEMT has been fabricated on Si that attains a significant advancement over HEMT configurations on bulk Si [94]. On the other hand, GaN HEMTs have also been established on semi-insulating SiC for HP generation using field-plated gates [95].

Note that, for power applications, normally-on GaN HEMTs are problematic, and that normally-off GaN HEMTs offer much higher performance. For this reason, normally-off GaN HEMT switches, as shown in Fig. 15 [96], are readily finding applications in power systems, where the AlGaN layer under the very narrow gate region produces a positive threshold voltage. Normally-off GaN HEMT structures can be produced a different way using a fluorine-based plasma treatment of the gate region instead of the narrow gate region of AlGaN configuration [97]. As a result, the threshold voltage is achieved via plasma treatment that incorporates fluorine ions in the AlGaN barrier. An arrangement of the gate recess together with a fluorine-based surface treatment of normally-off AlGaN/GaN HEMTs has been a proven solution for obtaining high performance [98]. In addition, a normally-off p-n gate HEMT can also be utilized in a 2DEG depletion layer for observation, as shown in Fig. 16.

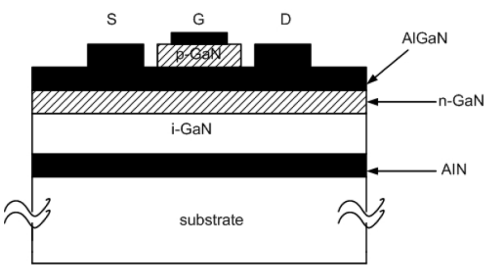

Fig. 16. *Schematic of a p-n gate GaN HEMT [99].*

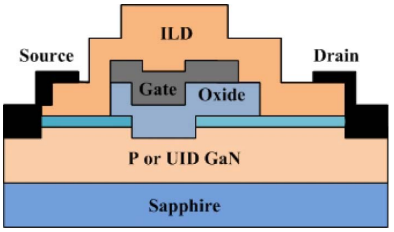

Fig. 17. *Schematic of a lateral GaN hybrid MOS-HEMT [100].*

Generally, lateral GaN MOSFETs show outstanding performance in normally-off operation and large conduction band offset for HP applications. In this case, a large conduction band offset has some reliability problems and less susceptibility that inject hot electrons, in particular, those related to surface and current collapse—this makes them an alternative to SiC MOSFET and GaN HEMTs [9], [100]. In the case of SiC MOSFETs, the presence of interface states limits the performance. To overcome these limitations, GaN MOSFETs can be designed by incorporating the AlGaN/GaN heterostructure into the reduced surface field (RESURF) region, as shown in Fig. 17.

C. GaN Cascode Configurations

The basic GaN HEMT structure is typically an ON-state device [20], [101], [102]. In order to increase its performance and applicability, manufactures are using the cascode configuration to obtain normally OFF-state behavior. The commercially available cascode configuration typically has a voltage rating of around 600 V and is constructed using a conventional MOSFET and a high-voltage depletion GaN [103]. As an example, the depletion mode (D-Mode) GaN HEMT device is connected in series with low-voltage (LV) Si MOSFET (normally, 30 V and low ON-state resistance), as shown in Fig. 18. The cascode structure results in an enhancement switch by applying the voltage pulse on the LV Si MOSFET gate in order to regulate the high-voltage D-Mode GaN HEMT to turn on and off [83], [104], [105]. When the gate is in the ON-state condition, the GaN HEMT channel

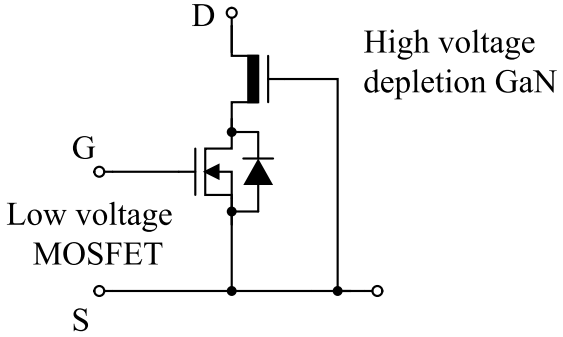

Fig. 18. *GaN cascode configuration.*

Table 5 Ratings of GaN Switch in TO-220 Package (TPH3006PS)

Parameters	Min	Typical	Max	Test Conditions
Maximum Drain-Source Volt-age ($V_{\mathrm{DSS-MAX}}$)	600 V	-	-	$V_{\mathrm{GS}} = 0$ V
Gate Threshold Voltage ($V_{\mathrm{GS(th)}}$)	1.35 V	1.8 V	2.35 V	$V_{\mathrm{DS}} = V_{\mathrm{GS}}$, $I_{\mathrm{D}} = 1$ mA
Drain-Source On-Resistance, $R_{\mathrm{DS(on)}}$ at $T_j = 25°\mathrm{C}$	-	0.15 Ω	0.18 Ω	$V_{\mathrm{GS}} = 8$ V, $I_{\mathrm{D}} = 11$ A, $T_j = 25°\mathrm{C}$
Drain-Source On-Resistance, $R_{\mathrm{DS(on)}}$ at $T_j = 175°\mathrm{C}$	-	0.33 Ω	-	$V_{\mathrm{GS}} = 8$ V, $I_{\mathrm{D}} = 11$ A, $T_j = 175°\mathrm{C}$
Drain-to-Source Leakage Current, $I_{\mathrm{DSS(on)}}$ at $T_j = 25°\mathrm{C}$	-	2.5 μA	90 μA	$V_{\mathrm{DS}} = 600$ V, $V_{\mathrm{GS}} = 0$ V, $T_j = 25°\mathrm{C}$
Drain-to-Source Leakage Current, I_{DSS} at $T_j = 150°\mathrm{C}$	-	10 μA	-	$V_{\mathrm{DS}} = 600$ V, $V_{\mathrm{GS}} = 0$ V, $T_j = 150°\mathrm{C}$
Gate-to-Source Forward Leakage Current, I_{GSS}	-	-	100 nA	$V_{\mathrm{GS}} = 18$ V
Gate-to-Source Reverse Leakage Current, I_{GSS}	-	-	-100 nA	$V_{\mathrm{GS}} = -18$ V
Input Capacitance, C_{ISS}	-	740 pF	-	$V_{\mathrm{GS}} = 0$ V, $V_{\mathrm{DS}} = 100$ V, $f = 1$ MHz
Output Capacitance, C_{OSS}	-	133 pF	-	$V_{\mathrm{GS}} = 0$ V, $V_{\mathrm{DS}} = 100$ V, $f = 1$ MHz
Reverse Transfer Capacitance, C_{RSS}	-	3.6 pF	-	$V_{\mathrm{GS}} = 0$ V, $V_{\mathrm{DS}} = 100$ V, $f = 1$ MHz
Turn-On Delay, $t_{\mathrm{d(on)}}$	-	4 ns	-	$V_{\mathrm{DS}} = 480$ V, $V_{\mathrm{GS}} = 0 - 10$ V, $I_{\mathrm{D}} = 11$ A, $R_{\mathrm{G}} = 2$ Ω
Rise Time, t_r	-	3 ns	-	$V_{\mathrm{DS}} = 480$ V, $V_{\mathrm{GS}} = 0 - 10$ V, $I_{\mathrm{D}} = 11$ A, $R_{\mathrm{G}} = 2$ Ω
Turn-Off Delay, $t_{\mathrm{d(off)}}$	-	10.5 ns	-	$V_{\mathrm{DS}} = 480$ V, $V_{\mathrm{GS}} = 0 - 10$ V, $I_{\mathrm{D}} = 11$ A, $R_{\mathrm{G}} = 2$ Ω
Fall Time, t_f	-	3.5 ns	-	$V_{\mathrm{DS}} = 480$ V, $V_{\mathrm{GS}} = 0 - 10$ V, $I_{\mathrm{D}} = 11$ A, $R_{\mathrm{G}} = 2$ Ω

path can permit current in both directions because it does not have any internal body diode. The conduction loss only occurs in the GaN HEMT due to low ON-state resistance of the LV Si MOSFET.

In most cases, the MOSFET body diode in a boost [106], [107], buck, or BB converter [108], [109] does not conduct current. In the case of a MOSFET body diode in an HB inverter, it can only conduct current with complementary gating pulses. The MOSFET body diode produces high conduction losses during the large dead-band time. The short dead-band time in GaN switches produces low conduction losses, which may be negligible. In addition, the MOSFET body diode may recover at near ZVS during the turn-on condition [110].

1) Gate Resistor: The GaN switch can be turned on or off by controlling the gate of the LV MOSFET. Generally, the gate resistor is used to control the switching time interval to turn on and off the MOSFET. The low switching losses are obtained due to LV MOSFET. Therefore, unlike the Si-MOSFETs, the gate resistance of the GaN switch plays a negligible role in the switching performance. In addition, the manufacturers have recommended using a driving GaN switch without connecting any gate resistor [101].

2) GaN Switch Characterization: The datasheet specifications of the GaN switch used in this article are tabulated in Table 5. The GaN switch is in a TO-220 package. The GaN device characterization is vital for predicting its switching and conduction losses. This is essential when designing and analyzing the thermal characteristics of a power converter to calculate its efficiency. Usually, device manufacturers provide several loss curves that are either theoretical or experimental, under different operating conditions [111]. It is, therefore, required to confirm the thermal and device characteristics experimentally before using them.

The basic GaN switch schematic circuit diagram of ON-state device characterization is shown in Fig. 19. To turn on the GaN switch, a small duration of gate pulse can be applied through the switch. The conduction voltage drop ($V_{\mathrm{DS(ON)}}$) and the drain current (I_{D}) can be measured across the source to drain terminal. The experimental results can be presented at several junction temperature (T_j), where GaN switch will be heated up to desired temperature using a heating resistor. The ON-state resistance ($R_{\mathrm{DS(ON)}}$) at the operating temperature (T_c) and the drain current (I_{D}) can be expressed as

$$R_{\mathrm{DS(ON)}} = \frac{V_{\mathrm{DS(ON)}}}{I_{\mathrm{D}}}. \tag{1}$$

It is strongly recommend that the measure ON-state resistance ($R_{\mathrm{DS(ON)}}$) characteristics depends on the junction temperature and does not depend on the drain current.

IV. WBG POWER DC–DC CONVERTER TOPOLOGIES

Renewable energy sources, such as solar PV, are a promising alternative for clean and efficient energy production. Renewable energy sources are probably the most demanding of all distributed power generation. However, it is necessary to set strict limits on the amount of ripple current, common-mode voltage, and load variations. The

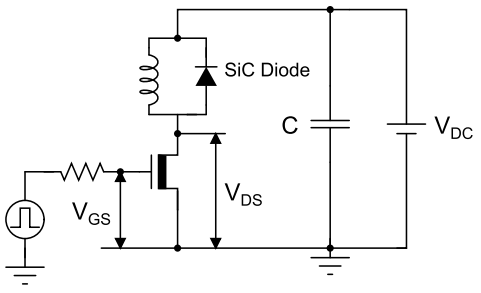

Fig. 19. *GaN characterization setup.*

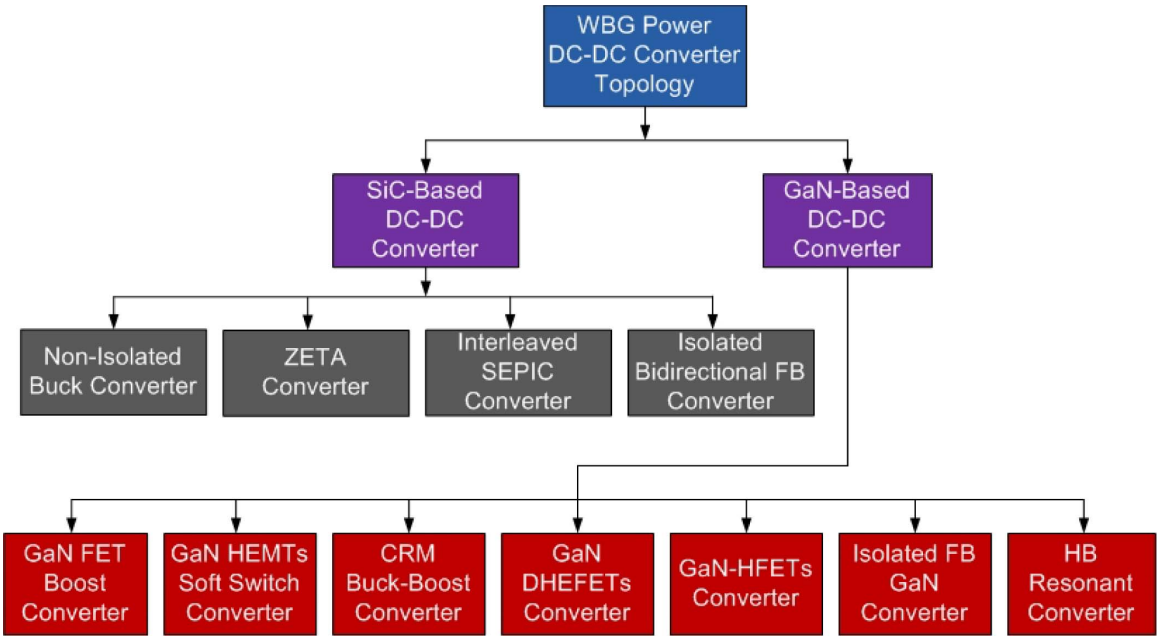

Fig. 20. ***Classification of WBG power dc–dc converter topologies.***

typically low output voltage from a renewable sources stack needs to be boosted to a higher voltage level for grid interfacing [112], [113]. Thus, there is a need for high-efficiency power converters and, in the case of LV, high current and galvanic isolation. It is worth noting that the implementation of such converters is not a trivial task. The favorable characteristics of these dc–dc converters are cost, reliability, wide input range, flexibility, scalability, and efficiency [113], [114]. Of these, scalability can refer to the different power ratings and the ability to select a design topology that results in lower losses and less stress on the converter's components in terms of the maximum voltage or current values. Note that there are two types of losses seen in power semiconductors: 1) static losses that occur due to finite response time that a device takes in response to an applied voltage and 2) conduction losses are a function of the voltage drop across the device and the current passing through it. For LV high-current applications, conduction losses dominate [115], [116].

However, commercial interest in WBG power devices has been increasing over the last decade due to their high breakdown voltage, high temperature, high-efficiency, and HF operation for clean and efficient energy production. Note that WBG power dc–dc converter topologies can be classified into SiC- and GaN-based dc–dc converters, as shown in Fig. 20, where Table 6 shows a performance comparison of these topologies to provide some qualitative assessment. As an example, several types of WBG-based HF HP dc–dc converter topologies are shown in Figs. 21–31, such as: 1) a GaN FET and SiC Schottky diode-based

Table 6 Performance Comparisons of SiC- and GaN-Based DC–DC Converter Topologies [13]–[15], [104], [117]–[123]

Parameters	SiC-based converter topologies	GaN-based converter topologies
Switching speed	Lower	Higher
Switching frequency	Lower	Higher
Power loss	Lower	Higher
Power density	Medium	Higher
Converter size	Medium	Smaller
Operating temperature	Higher	Higher
Discharge	Lower	Higher
Filter component	Resonable	Light
Voltage stress	Medium	Lower
Voltage drop on active devices	Medium	Lower
Control mechanism	Easier	Compex
Control variable	Multiple	Multiple
Complexity	Less	Higher
Necessity switching device	Less	Lower
Efficiency	Lower	Higher

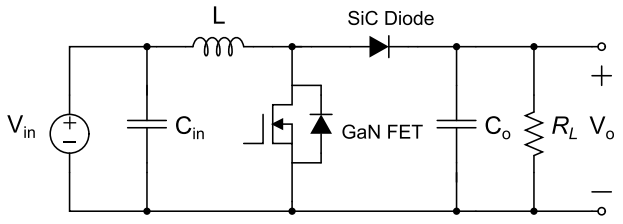

Fig. 21. *Schematic of 1:2 boost converter using GaN FET and SiC Schottky diodes. A dynamic load was used to hold the output current at 0.5 A while ramping the output voltage to 360 V [13].*

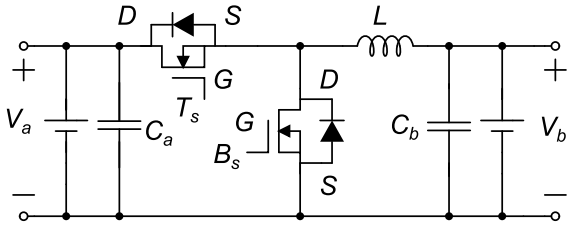

Fig. 23. *GaN-based CRM (GaN CRM) bidirectional BB converter [15].*

boost converter; 2) a GaN HEMTs SS converter; 3) a critical current mode (CRM) bidirectional BB converter; 4) a double-heterostructure FET (DHEFET) converter; 5) a high breakdown voltage GaN heterojunction-field-effect transistor (GaN-HFET); 6) a GaN isolated FB converter; 7) GaN-based HB resonant converter for speed control of a brushless dc (BLDC) motor; 8) a nonisolated dc–dc buck converter; 9) an SiC Schottky/GaN E-HEMT-based dc–dc ZETA converter; 10) an SiC-cascode-based Interleaved dc–dc SEPIC converter; and 11) an SiC-based isolated bidirectional dc–dc converter.

A. GaN FET and SiC Schottky Diode-Based Boost Converter

In [13], a 360-V/180-W boost converter was proposed using GaN FET and SiC Schottky diodes at 200-kHz switching frequency, with an efficiency of >92%, as shown in Fig. 21. The converter was built with normally-off GaN-on-Si HEMTs that allow to high breakdown voltage ($V_B >$ 1100 V), low-leakage current (<10 μA/mm at $V_B/2$), highest peak current $I_{\max} = 5$ A, and the highest $V_B^2/R_{\text{on,sp}}$ ratio of 272 MW/cm^2. These values are reasonable for a normally-off GaN-on-Si device. Table 7 shows the performance summarized of a 1:2 boost converter for a normally-off GaN-on-Si device compared to an Si IGBT device [13].

B. GaN HEMT-Based SS Class-Φ_2 Converter

A Class-Φ_2 converter topology that uses a GaN HEMT as soft-switching devices is shown in Fig. 22 [117], which has been utilized in HP applications under zero-voltage/zero-current conditions with very high-speed switching range in the HF-to-VHF range [117]. The converter switching loss is function of capacitance, voltage, and frequency, a decrease in any of these parameters leads to reduced loss. For verification, datasheet parameters (typical) for the GaN device are used from every manufacturer with commercially available voltage ratings over 600 V_{DS}. The selected GaN package GS66504B HEMT has the best combination of the drain–source ON-resistance ($R_{\text{DS,ON}}$), the output capacitance (C_{OSS}), and the input capacitance (C_{ISS}) for the planned family of converters. The performance comparison of GaN package GS66504B HEMT model is shown in Table 8 [117].

C. GaN-Based CRM Bidirectional Buck-Boost Converter

The GaN-based CRM bidirectional BB converter with an inverse coupled inductor is shown in Fig. 23, which can be continuously driven at high switching frequency (MHz range) with low switching loss and driving loss, and also is more compact in physical size [15]. The advantage of the inverse coupled inductor is a reduced resonant time period in CRM compared to a noncoupled inductor with also improved SS and circulating energy when the duty cycle is less than 50% and greater than 50%, respectively.

D. E-Mode GaN Double-Heterostructure FET (GaN DHEFET) Boost Converter

Fig. 24 shows a 100-W Enhancement-mode (E-mode) GaN DHEFET boost converter. For switching applications, E-mode GaN devices are usually preferred. Different concepts have been proposed in the literature [124] to convert

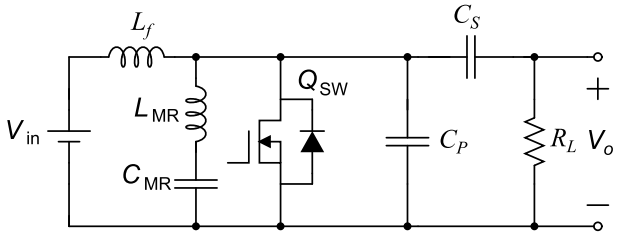

Fig. 22. *GaN-based HEMTs (GaN HEMTs) soft switch Class-Φ_2 converter [117].*

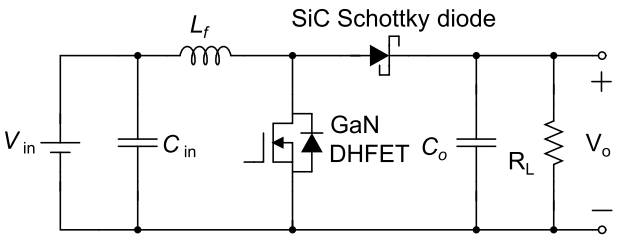

Fig. 24. *GaN DHEFET converter [14].*

Table 7 Performance Summarized of 1:2 Boost Converter for a Normally-off GaN-on-Si Device Compare to Si IGBT Device [13]

Parameters	Symbol	Value
Output power	P_o	180 W
Output voltage	V_o	360 V
Switching frequency	$f_{\rm sw}$	200 kHz
Breakdown voltage	V_B	>1100 V
Low-leakage current	i_c	$<10\ \mu$A/mm
High peak current	$I_{\rm max}$	5 A
Highest ratio	${V_B}^2/R_{\rm on,sp}$	272 MW/cm^2
Breakdown field	F_B	95 V/μm
Efficiency	η	>92%

the GaN device from the conventional D-mode to E-mode. Recently, E-mode devices have been proposed to obtain high-efficiency values of 96.1% and 93.9% at switching frequencies of 500 and 850 kHz, respectively [14]. The high potential of GaN-on-Si devices for HF power switching applications is compared with commercial Si-based MOSFET devices, as shown in Table 9 [14], [125].

E. IPT-ZVS Converter Using GaN Heterojunction-Field-Effect Transistor

Mishima and Morita [118] proposed a novel zero-voltage soft-switching bridgeless active rectifier-based multiresonant dc–dc power converter while using a high breakdown voltage GaN-HFET for an inductive power transfer (IPT) system, as shown in Fig. 25. This converter obtains high efficiency due to low switching losses and normally-off operation is shown in a test of a 700-W converter while comparing its performance with super junction MOSFET (SJ MOSFET)-based converter. Table 10 compares GaN-HFET and SJ MOSFET devices [118].

F. Isolated FB DC–DC GaN Converter

Fig. 26 shows the GaN FET isolated FB converter, which is attractive for synchronous rectification with a high-efficiency value of 98.8%. Moreover, GaN-based FETs can achieve high-efficiency power conversion even with hard switching topologies. Unlike Si MOSFETs, GaN-based FETs have no reverse recovery losses because no minority carriers are engaged in reverse diode conduction [104], [126]. On the other hand, a high forward voltage drop occurs due to forward diode conduction losses. These losses can be minimized by properly selecting the duty cycle of each of the switches. The GaN device packages, EPC2010C and EPC2001C, are used in an FB converter for the primary and secondary side switches, respectively, with a breakdown voltage of 200 and 100 V, respectively. Table 11 shows the performance comparison of GaN FET with alternative Si MOSFET [104].

Table 8 Performance Comparison of GaN Package GS66504B HEMT Model at Several Frequencies [117]

Parameters	10 MHz	30 MHz	54.24 MHz
$P_{\rm IN}$	1185 W	1046 W	1003 W
η	94.5%	93.5%	93.5%
$I_{\rm RMS}$	10.9 A	9.6 A	10.9 A
$P_{\rm DISS}$	5.4 W	10.5 W	17.1 W
$V_{\rm DS,MAX}$	603 V	606 V	540 V

Table 9 E-Mode GaN DHEFET-Based Converter Specifications and Efficiency Demonstrated at Several Switching Frequencies Compared to Commercial Si-Based MOSFET Devices [14], [125]

Parameters	Symbol	Value
Output power	P_o	100 W
Drain-source voltage	$V_{\rm DS}$	140 V
Total gate charge	Q_G	11 nC
Drain-source on-resistance	$R_{\rm DS,ON}$	2.5 Ω
Switching frequency	$f_{\rm sw}$	500 kHz and 850 kHz
Efficiency	η	96.1% and 93.9%
Rise time	t_r	5 ns
Fall time	t_f	20 ns

G. GaN-Based HB Resonant Converter for BLDC Motor

A GaN-based HB resonant converter has been proposed at 100-kHz operating switching frequency for BLDC [119], as shown in Fig. 27. This proposed converter uses GaN FETs switches instead of Si-based switches, which realizes an SMPS with compact size. The use of GaN switches not only reduces the size of the converter but also works efficiently compared to Si-based counterparts. A resonant circuit is also engaged in this arrangement, which confirms ZVS and ZCS to reduce the voltage and current stresses on GaN switches. Table 12 shows a comparison between GaN FET and traditional Si-based MOSFET [119].

H. Nonisolated DC–DC Buck Converter Based on Si-MOSFET, SiC-JFET, and GaN-Transistor

A nonisolated dc–dc buck converter is shown in Fig. 28 [120], which is designed by using Si-MOSFET, SiC-JFET, and GaN devices for industrial application. Note that manufactures fabricated SiC devices for both lower

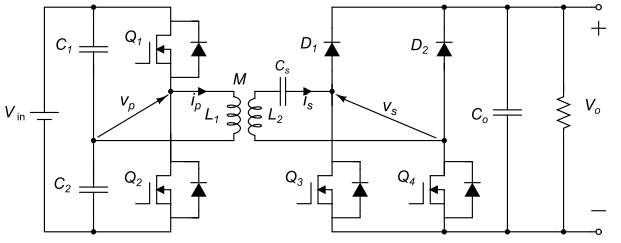

Fig. 25. *IPT-ZVS converter using GaN-HFET [118].*

Table 10 Performance Activities of GaN-HFET and SJ-MOSFET in Comparison [118]

Parameters	Symbol	GaN-HFET PGA26C09DV (panasonic)	SJ-MOSFET IXKC-15N60C5 (IXYS)
Drain-source voltage	$V_{\rm ds}$	600 V	600 V
Drain current	I_d	15 A	15 A
Gate threshold voltage	$V_{\rm th}$	1.2 V	3.0 V
Drain-source on-resistance	$D_{\rm ds,on}$	71 mΩ	150 mΩ
Gate charge	Q_g	9 nC	40 nC
Input capacitance	$C_{\rm iss}$	115 pF	1100 pF
Output capacitance	$C_{\rm oss}$	80 pF	70 pF
Dead time interval	t_d	500 ns	500 ns

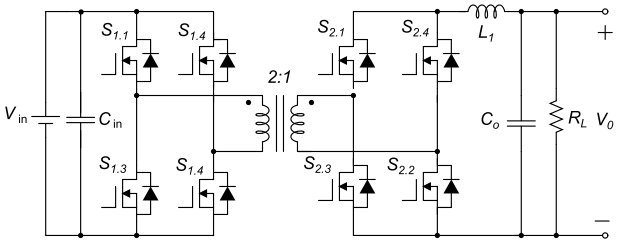

Fig. 26. *GaN-based isolated FB dc–dc step down converter [104].*

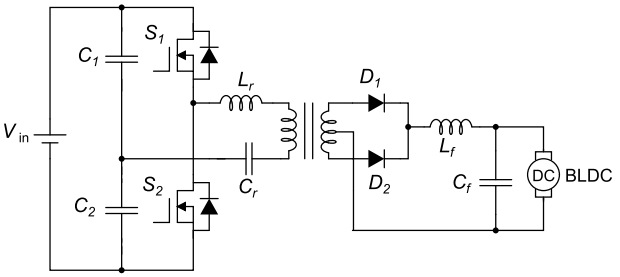

Fig. 27. *GaN-based HB resonant converter for the BLDC motor [119].*

and higher voltage range, while the GaN devices are fabricated for lower voltage range. However, the LV WBG power devices show outstanding performance compared to conventional Si-based power devices. They operate with a gate voltage ($V_{\rm GS}$) of +25 and −25 V that are applied to turn on and off the Si-MOSFET, whereas a gate voltage of +3 and −15 V is supplied to turn on and off an SiC-JFET. On the other hand, a gate voltage +6 and 0 V is used to turn on and off a GaN transistor.

In addition, the switching energy losses for Si-MOSFET during turn-on and turn-off conditions are 218.72 and 6.0312 μJ, respectively, while switching energy losses for SiC-JFET during turn-on and turn-off conditions are 26.731 and 12.058 μJ, respectively. The switching energy losses for the GaN-transistor are 17.987 and 8.1175 μJ during the turn-on and turn-off conditions, respectively. Table 13 shows a performance comparison of several power devices [120].

Note that the design requirements depend on the size of the power converter and power density by many applications [127]. The selection of switching frequency is most important for the converter to operate the power switches with high efficiency. This is because converter switching loss depends on the selection of switching frequency, where high switching frequency leads to higher switching loss. On the other hand, the high switching frequency can result in smaller reactive components, facilitating integration and leading to a more compact converter. The total power loss and overall efficiency are calculated for several power devices with 20–200-kHz switching frequency at a junction temperature of 150 °C, as shown in Table 14 [120]. It is clear that the power loss of the converter dramatically increases with increasing switching frequency, resulting in a degradation of the overall efficiency. According to the

Table 11 Performance Comparison of GaN FET With Alternative Si MOSFET [104]

Device (package)	GaN FET (LGA)	Si MOSFET #1 (Power56)	Si MOSFET #2 (SuperS08)
Area ($\rm mm^2$)	6.6	31.7	30.9
$R_{\rm DS(on)}$(mΩ)	5.6	3.3	4
Drain-source on-resistance, $R_{\rm DS(on)} \times$ Area ($\rm m\Omega \cdot m^2$)	37	105	124
Input capacitance, $C_{\rm iss}$(pF)	770	2945	2320
Output capacitance, $C_{\rm oss}$(pF)	430	1730	1070
Output charge, $Q_{\rm oss}$ (nC)	31	123	120
Output reverse recovery charge, $Q_{\rm oss}$ (nC)	0	57	76

Table 12 Comparison of GaN FET and Si MOSFET [119]

Parameters	GaN FET (GS66508T)	Si-MOSFET (Infineon SPP20N60CFD)
V_o	12 V	12 V
I_o	1.5 A	1.5 A
η	93.87%	71.63%
Power loss	1.19 W	6.62 W
Temperature	41.6°C	62.5°C
R_{DS}	0.05 Ω	0.22 Ω
Input capacitance	260 pF	2400 pF
Output capacitance	65 pF	780 pF
Parasitic inductance	10 nH	150 nH

analysis of the total power losses, the GaN-based converter provides the best performance efficiency. Noted that the efficiencies of Si-MOSFET, SiC-JFET, and GaN-transistor-based converter are 96%, 97.85%, and 98.25%, respectively, up to a 20-kHz switching frequency.

I. SiC Schottky/GaN E-HEMT-Based DC–DC ZETA Converter

In [121], a dc–dc ZETA converter was proposed for high step-up applications by using a Schottky/GaN E-HEMT device, as shown in Fig. 29. This converter can perform with continuous output current and noninverting output voltage.

For performance evaluation, several types of semiconductor power devices, such as Si-MOSFET (R6047ENZ1), SiC Schottky diode (CPW5-0650-Z030B), and GaN E-HEMT (GS66506T), are integrated into this converter. During the test condition, the Si-MOSFET/SiC Schottky diode is turned on with +15 V and turned off with −15 V at the gate, while the turn-on gate voltage of +6 V and the turn-off gate voltage of 0 V are used for the GaN E-HEMT/SiC Schottky diode. The overall efficiencies using these devices are 96.186% and 98.082% for the Si-MOSFET/SiC Schottky diode and the GaN E-HEMT/SiC Schottky diode, respectively, at 48-V input voltage. Table 15 shows the performance comparison of dc–dc ZETA converters based on several semiconductor power devices [121].

J. SiC-Cascode-Based Interleaved DC–DC SEPIC Converter

Typically, interleaved SEPIC converters can be broadly used in renewable power generation systems, including

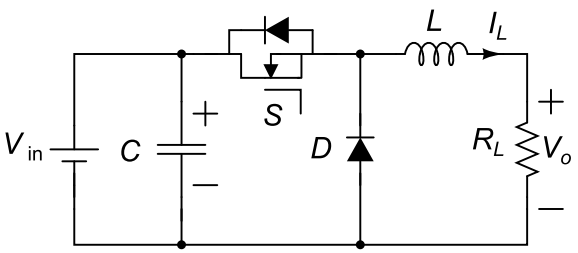

Fig. 28. *Nonisolated dc–dc buck converter [120].*

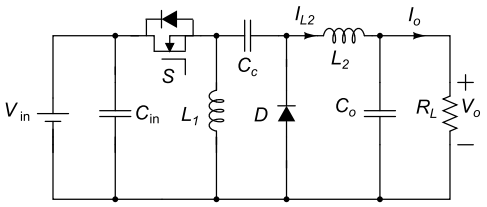

Fig. 29. *SiC Schottky/GaN E-HEMT-based dc–dc ZETA converter [121].*

PV and fuel cells, which are facing the critical problems of high-input current ripples and varying low-output voltages. These problems can be overcome by applying the interleaved SEPIC converter, as shown in Fig. 30 [122]. The interleaved method is well-recognized, which is applied to dc–dc converters in order to generate more power and reduce the harmonic distortion. In order to evaluate the performance of Si-MOSFET/Si-diode and SiC-JFET/SiC-Schottky diode power devices, the interleaved dc–dc SEPIC converter is integrated with these power devices and with a rated power of 600 W and input and output voltages of 100 and 400 V, respectively. The performance comparison based on Si-MOSFET/Si-diode and SiC-JFET/SiC-Schottky power devices is shown in Table 16 [122].

K. SiC-Based Isolated Bidirectional DC–DC Converter

During recent progress development in the area of semiconductor devices, the SiC MOSFET has attracted growing attention. In comparison to traditional Si MOSFETs, the SiC MOSFET has a high blocking voltage capability, low ON-state resistance, and short turn-on/turn-off times. An SiC-based 1200-V/110-V isolated bidirectional dc–dc converter topology is shown in Fig. 31 [123]. In this converter, the 3L FB structure is used on the primary side, which can make the switching device tolerate half of the input voltage. A full-wave rectifier is used on the secondary side, which can reduce the loss and ensure the bidirectional flow of the system. In order to avoid switching overlap within the primary side of the converter, a dead-band time is fixed between S_1 and S_3, S_2 and S_4, S_5 and S_7, and S_6 and S_8

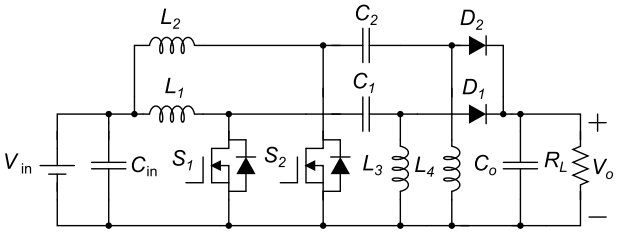

Fig. 30. *Interleaved dc–dc SEPIC converter based on SiC-cascode power devices [122].*

Table 13 Performance Comparison of Power Devices [120]

Parameters	Si-MOSFET (R6020PNJ)	SiC-JFET (UJN1205Z)	GaN-transistor (GS66516B)
Breakdown voltage (V)	600	1200	650
Rated current (A)	20	38	60
Junction temparature (°C)	150	175	150
Switching energy losses during turn-on and turn-off (μJ)	218.72 and 6.0312	26.731 and 12.058	17.987 and 8.117
Gate-source voltage during turn-onn and turn-off (V)	+25 and -25	+3 and -15	+6 and 0
Gate resistance (Ω)	13.4	5	5

Table 14 Power Loss and Efficiency Calculated by Using Various Power Devices With 20–200-kHz Switching Frequency at the Junction Temperature of 150 °C [120]

Parameters	Si-MOSFET/Si-diode based converter		SiC-JFET/SiC-Schottky diode based converter		GaN-transistor/SiC-Schottky diode based converter	
Switching frequency (kHz)	power loss (W)	efficiency (%)	power loss (W)	efficiency (%)	power loss (W)	efficiency (%)
20	9.41	96	5.19	97.85	4.92	98.25
80	21.72	91	7.57	97	6.63	97.23
140	37.61	87	10	95.75	8.34	96.85
200	52.64	83	12.46	95	10.07	96

switches, while the switching pulses of the secondary side adopt a synchronous rectification approach [123].

L. Proposed GaN-Based DC–DC Step-Up Converter With a Voltage-Lift Switched-Inductor Circuit

In this article, an HF and HV gain GaN-based transformerless dc–dc step-up converter with a voltage-lift switched-inductor circuit is proposed, as shown in Fig. 32. The proposed converter permits an increase in the switching frequency and also high efficiency and high voltage gain due to small switching losses. The control strategy is improved to allow two independent switching frequencies: one of which operates at a high switching frequency up to the megahertz (MHz) range to reduce the size of the converter components, and the other one operates at a relatively low switching frequency to obtain minimum output voltage ripple. The converter is

Table 15 Performance Comparison of the DC–DC ZETA Converter Based on Several Semiconductor Power Devices [121]

Parameters	Si-MOSFET/SiC Schottky diode (R6047ENZ1)	GaN E-HEMT/SiC Schottky diode (GS66506T)
Breakdown voltage (V)	600	650
Rated current (A)	47	22.5
Junction temparature (°C)	150	150
Switching energy losses during turn-on and turn-off (μJ)	44.219 and 23.317	24.15 and 7.77
Gate-source voltage during turn-on and turn-off (V)	+15 and -15	+6 and 0
Gate resistance (Ω)	5	5
Overall efficiency (%) at $f_{sw} = 100$ kHz, and $V_{in} = 48$ V	96.186	98.082

Table 16 Performance Comparison Based on Si-MOSFET/Si-Diode and SiC-JFET/SiC-Schottky Diode Power Devices [122]

Parameters	Si-MOSFET/Si-diode (R6535ENZI)	SiC-JFET/SiC-Schottky diode (UJC06505K)
Blocking voltage (V)	650	650
Rated current (A) at $T_j = 25°C$	35	36.5
Maximum junction temparature (°C)	150	150
Drain-source on-resistance ($R_{DS,on}$) at $T_j = 25°C$	98 mΩ	34 mΩ
Gate resistance (Ω) at $T_j = 25°C$	10	20
Gate-source voltage during turn-on and turn-off (V)	+20 and -20	+12 and 0
Switching energy losses during turn-on and turn-off (μJ)	102.5 and 165.7	130.8 and 43.2
Power loss (W) at $T_j = 25°C$	14.6	10.4
Overall efficiency (%) at $f_{sw} = 50$ kHz, and $V_{in} = 100$ V	95	97.5

Table 17 Performance Comparison of the Proposed DC–DC Converter Topology With Several Other WBG Power DC–DC Converter Topologies

Topologies	P_o (W)	f_{sw} (MHz)	η (%) (For GaN device)	η (%) (For SiC device)	V_{in} (V)	V_o (V)	Duty cycle (%)	Dead-time (μs)
Converter in [13]	180	0.2	>92	N/A	N/A	360	N/A	N/A
Converter in [14]	100	0.5	96.1	N/A	N/A	140	50	N/A
Converter in [15]	N/A	1	98.5	N/A	150 and 380	380 and 150	>50	N/A
Converter in [104]	2400	0.05	98.5	N/A	130	50	<50	N/A
Converter in [117]	1000	54.24	93.5	N/A	250	N/A	>50	N/A
Converter in [118]	700	0.085	93.4	N/A	230	130	>50	0.5
Converter in [119]	N/A	0.1	93.87	N/A	40	12	N/A	0.004
Converter in [120]	280	0.02	98.25	97.85	140	48	N/A	N/A
Converter in [121]	N/A	0.1	98.082	97.450	48	400	N/A	N/A
Converter in [122]	600	0.05	N/A	97.5	100	400	N/A	N/A
Converter in [123]	N/A	0.03	N/A	N/A	1200	110	N/A	0.02
Converter in [128]	500	0.05	96	93.50	120	210	N/A	0.1
Proposed converter	420	0.01 and 6	98.23	N/A	50	650	50	0.3 and 0.005

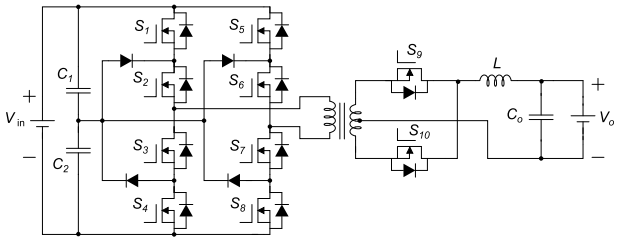

Fig. 31. *SiC-based isolated bidirectional dc–dc converter [123].*

demonstrated through the design of a 420-W high voltage gain, with a maximum voltage multiplication, $M_v = 13$, resulting in $V_o = 650$ V for a 50-V input. The simulated peak efficiency for this structure is 98.23% at 420 W, as shown in Fig. 33. These results are compared with published converter's performance, as shown in Table 17.

V. DESIGN RECOMMENDATION AND FUTURE TRENDS

To enable the development of a high-efficiency power supply on-chip, a number of research challenges need to be overcome, as follows.

A. Inaccurate Switching Models

Proper switching models that incorporate quiescent bias and frequency-dependent trap models need to be developed for proper simulation and design work. The characterization for the modeling needs to be carried out using pulsed IV techniques. One of the major challenges with design in a GaN process is the devices are D-Mode n-type. The lack of p-type devices makes the design of complex logic circuits challenging. Hence, the design of complex analog circuitry is challenging; however, circuit design approaches that have already been developed in GaAs designs can be applied.

B. Optimization of the Power Switch

A significant criterion for evaluating the quality of a power device is thermal performance in end-system applications. It is well known that thermal problems severely constrain converter performance requirements, such as ripple and harmonic distortion. The problem is exacerbated when operating at a high switching speed and higher output power levels. In order to design HF, high-efficiency and high-voltage power switches' accurate circuit and thermal modeling are needed since the proper sizing of source–drain metallization is critical. The layout with proper thermal vias to extract the generated heat away from the chip surface must also be modeled. This modeling

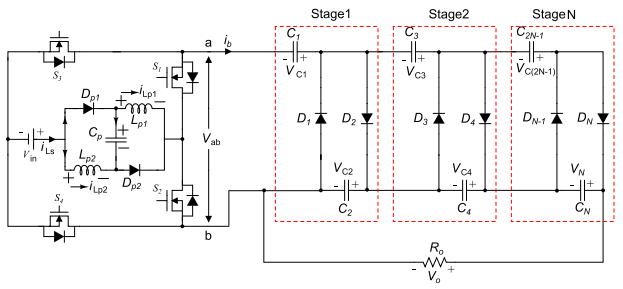

Fig. 32. *Proposed GaN-based transformerless dc–dc step-up converter with a voltage-lift switched-inductor circuit.*

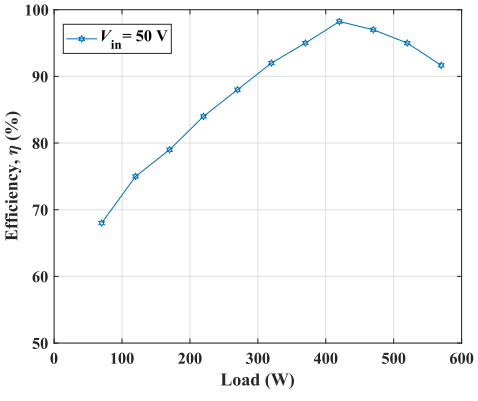

Fig. 33. *Measured simulated peak efficiency versus load of the proposed converter.*

is critical for accurate estimation of the quality of a power device, as excessive heating can severely limit the overall performance of the integrated converter in terms of output ripple, harmonic distortion, and so on. The problem is further exacerbated when operating at high switching speed and high output power levels and the need for special cooling mechanisms to limit chip heating [128], [129].

C. Codesign of Mixed-Signal Circuits and Custom Design Flows

The design of mixed-signal circuits in GaN is very challenging since most of the circuits designed are tailored toward RF or for power switching. There is a significant knowledge gap in how the circuits interact due to spikes that may be caused by the high-voltage switching. A combination of schematic design, mixed-signal simulation, layout, and layout extraction (dc, RF, time domain, and EM) analysis will have to be combined to fully understand all the forces at play within the codesign environment.

D. Optimization of Control Circuits

One of the major challenges in implementing mixed-signal control circuits and high-voltage switches is the feature size and transconductance temperature dependence of the transistor. High-voltage devices usually have larger peripheries, hence drawing more current through them, while digital circuits work with minimal drain currents; hence, proper sizing of both analog and digital circuits needs to be fully investigated.

E. Integration of High-Voltage GaN With Logic Functionalities

The physical integration of mixed-signal circuitry with high-voltage power switches needs to be carefully examined. The layout must have separate probe points to independently test the separate logic functions without interfering with each other. Moreover, the on-chip thermal distribution profile must be modeled with all the functionalities operating within the same substrate and environment to give an understanding of the packaging requirements and thermal hotspots.

F. Testing and Packaging

The fabricated structures need to be initially tested on-wafer to determine the yield within the die and then diced for packaging. The on-wafer test will include functional testing of all the mixed-signal circuitry and the high-voltage switch. The diced chips can be placed onto a high thermal conductivity carrier substrate and glued onto a package, which can be ceramic, metal, or plastic. Measurements can then be conducted to optimize the devices to minimize parasitics from the bonding wires and leads that form part of the chip interface to the external world. The packaged chipset can be measured for its performance and compared to simulated results. Test and measurement setups will be similar to an on-wafer setup, except that the chip is mounted on a prototype PCB with good thermal conductivity to draw the heat away from thermal bottlenecks.

VI. CONCLUSION

Notably, dc–dc converter topologies are commonly used in renewable energy, HV direct current (HVdc), medium-voltage direct current (MVdc), aerospace, automobile, and many other industries. This article presents an overview of the classical and recent development in power dc–dc converter topologies based on WBG semiconductor devices. The properties of WBG devices motivate a new generation of high-efficiency converters in applications where classical power converters present significant limitations, such as high-voltage, high-temperature, and HF operation. In addition, WBG devices and suitable circuit topologies are ideal specifically in HP density mobile applications, such as aerospace and EVs. The outstanding performance of HEMTs fabricated on GaN heterostructures has emerged in the last decade. The 2DEG together with high electron mobility makes these structures more attractive for high switching frequency applications. It can be concluded that advances in GaN-based dc–dc converters present promising solutions for obtaining high efficiency at higher switching frequencies with low power loss due to high carrier mobility in the 2DEG channel. ■

REFERENCES

[1] N. Ertugrul and D. Abbott, "DC is the future," *Proc. IEEE*, vol. 108, no. 5, pp. 615–624, May 2020.

[2] N. Bertoni, G. Frattini, R. G. Massolini, F. Pareschi, R. Rovatti, and G. Setti, "An analytical approach for the design of class-E resonant DC–DC converters," *IEEE Trans. Power Electron.*, vol. 31, no. 11, pp. 7701–7713, Nov. 2016.

[3] F. Pareschi, G. Setti, R. Rovatti, and G. Frattini, "Short-term optimized spread spectrum clock generator for EMI reduction in switching DC/DC converters," *IEEE Trans. Circuits Syst. I, Reg. Papers*, vol. 61, no. 10, pp. 3044–3053, Oct. 2014.

[4] F. Pareschi, N. Bertoni, M. Mangia, R. Rovatti, and G. Setti, "A unified design theory for class-E resonant DC–DC converter topologies," *IEEE Access*, vol. 7, pp. 83825–83838, 2019.

[5] N. M. L. Tan, T. Abe, and H. Akagi, "Design and performance of a bidirectional isolated DC–DC converter for a battery energy storage system," *IEEE Trans. Power Electron.*, vol. 27, no. 3, pp. 1237–1248, Mar. 2012.

[6] N. M. L. Tan, T. Abe, and H. Akagi, "Experimental discussions on operating frequencies of a bidirectional isolated DC-DC converter for a battery energy storage system," in *Proc. IEEE Energy Convers. Congr. Expo. (ECCE)*, Sep. 2013, pp. 2333–2340.

[7] W. Yu *et al.*, "High efficiency isolated DC-DC converter combining resonant and phase-shifted topologies for electrical vehicle chargers," in *Proc. 1st Int. Future Energy Electron. Conf. (IFEEC)*, Nov. 2013, pp. 175–180.

[8] D. Kahng, "A historical perspective on the development of MOS transistors and related devices," *IEEE Trans. Electron Devices*, vol. ED-23, no. 7, pp. 655–657, Jul. 1976.

[9] J. Millán, P. Godignon, X. Perpiñà, A. Pérez-Tomás, and J. Rebollo, "A survey of wide bandgap power semiconductor devices," *IEEE Trans. Power Electron.*, vol. 29, no. 5, pp. 2155–2163, May 2014.

[10] N. Kaminski and O. Hilt, "SiC and GaN devices–wide bandgap is not all the same," *IET Circuits, Devices Syst.*, vol. 8, no. 3, pp. 227–236, May 2014.

[11] R. Ramachandran and M. Nymand, "Analysis of capacitive losses in GaN devices for an isolated full bridge DC-DC converter," in *Proc. IEEE 11th Int. Conf. Power Electron. Drive Syst. (PEDS)*, Jun. 2015, pp. 467–472.

[12] S. Inoue and H. Akagi, "A bidirectional isolated DC–DC converter as a core circuit of the next-generation medium-voltage power conversion system," *IEEE Trans. Power Electron.*, vol. 22, no. 2, pp. 535–542, Mar. 2007.

[13] K. S. Boutros *et al.*, "Normally-off 5A/1100V GaN-on-silicon device for high voltage

applications," in *IEDM Tech. Dig.*, Dec. 2009, pp. 1–3, doi: 10.1109/IEDM.2009.5424396.
[14] J. Das *et al.*, "A 96% efficient high-frequency DC–DC converter using E-mode GaN DHFETs on Si," *IEEE Electron Device Lett.*, vol. 32, no. 10, pp. 1370–1372, Oct. 2011.
[15] X. Huang, F. C. Lee, Q. Li, and W. Du, "High-frequency high-efficiency GaN-based interleaved CRM bidirectional buck/boost converter with inverse coupled inductor," *IEEE Trans. Power Electron.*, vol. 31, no. 6, pp. 4343–4352, Jun. 2016.
[16] K. Shenai, "High-density power conversion and wide-bandgap semiconductor power electronics switching devices," *Proc. IEEE*, vol. 107, no. 12, pp. 2308–2326, Dec. 2019.
[17] B. J. Baliga, "Synopsis," in *The IGBT Device*. Norwich, NY, USA: William Andrew, 2015, ch. 20, pp. 667–676. [Online]. Available: http://www.sciencedirect.com/science/article/pii/B9781455731435000201
[18] M. Rahimo, "Future trends in high-power bipolar metal-oxide semi-conductor controlled power semi-conductors," *IET Circuits, Devices Syst.*, vol. 8, no. 3, pp. 155–167, May 2014.
[19] M. A. Briere, "GaN on Si based power devices: An opportunity to significantly impact global energy consumption," *CS MANTECH*, vol. 5, pp. 221–224, Feb. 2010.
[20] K. Shinohara *et al.*, "GaN-based field-effect transistors with laterally gated two-dimensional electron gas," *IEEE Electron Device Lett.*, vol. 39, no. 3, pp. 417–420, Mar. 2018.
[21] U. K. Mishra, S. Likun, T. E. Kazior, and Y.-F. Wu, "GaN-based RF power devices and amplifiers," *Proc. IEEE*, vol. 96, no. 2, pp. 287–305, Feb. 2008.
[22] B. Hughes, J. Lazar, S. Hulsey, D. Zehnder, D. Matic, and K. Boutros, "GaN HFET switching characteristics at 350V/20A and synchronous boost converter performance at 1 MHz," in *Proc. 27th Annu. IEEE Appl. Power Electron. Conf. Expo. (APEC)*, Feb. 2012, pp. 2506–2508.
[23] R. Pittini, A. Anthon, Z. Zhang, and M. A. E. Andersen, "Analysis and comparison of Si and SiC power devices on a grid-tie fuel cell energy storage system," in *Proc. Int. Power Electron. Appl. Conf. Expo. (PEAC)*, Nov. 2014, pp. 296–301.
[24] K. V. G. Raghavendra *et al.*, "A comprehensive review of DC–DC converter topologies and modulation strategies with recent advances in solar photovoltaic systems," *Electronics*, vol. 9, no. 1, pp. 1–41, 2020.
[25] M. Nymand and M. A. E. Andersen, "High-efficiency isolated boost DC–DC converter for high-power low-voltage fuel-cell applications," *IEEE Trans. Ind. Electron.*, vol. 57, no. 2, pp. 505–514, Feb. 2010.
[26] L. Xue, M. Mu, D. Boroyevich, and P. Mattavelli, "The optimal design of GaN-based dual active bridge for bi-directional plug-in hybrid electric vehicle (PHEV) charger," in *Proc. IEEE Appl. Power Electron. Conf. Expo. (APEC)*, Mar. 2015, pp. 602–608.
[27] E. A. Jones, F. F. Wang, and D. Costinett, "Review of commercial GaN power devices and GaN-based converter design challenges," *IEEE J. Emerg. Sel. Topics Power Electron.*, vol. 4, no. 3, pp. 707–719, Sep. 2016.
[28] E. Aklimi, D. Piedra, K. Tien, T. Palacios, and K. L. Shepard, "Hybrid CMOS/GaN 40-MHz maximum 20-V input DC–DC multiphase buck converter," *IEEE J. Solid-State Circuits*, vol. 52, no. 6, pp. 1618–1627, Jun. 2017.
[29] Q. Li *et al.*, "Technology road map for high frequency integrated DC-DC converter," in *Proc. 25th Annu. IEEE Appl. Power Electron. Conf. Expo. (APEC)*, Feb. 2010, pp. 533–539.
[30] W. H. Morman, M. H. Ramsey, and R. G. Hoft, "50-kW thyristor DC-to-DC converter," *IEEE Trans. Ind. Appl.*, vol. IA-8, no. 5, pp. 617–635, Sep. 1972.
[31] M. Nakaoka, N. Vietson, T. Maruhashi, and M. Nishimura, "High-power switching regulator type DC-DC converters controlled by time-sharing high-frequency thyristor choppers with energy-storage and-transfer reactors," *IEEE Trans. Magn.*, vol. MAG-15, no. 6, pp. 1794–1796, Nov. 1979.
[32] R. W. A. A. De Doncker, D. M. Divan, and M. H. Kheraluwala, "A three-phase soft-switched high-power-density DC/DC converter for high-power applications," *IEEE Trans. Ind. Appl.*, vol. 27, no. 1, pp. 63–73, Feb. 1991.
[33] J. Rodríguez, S. Bernet, B. Wu, J. O. Pontt, and S. Kouro, "Multilevel voltage-source-converter topologies for industrial medium-voltage drives," *IEEE Trans. Ind. Electron.*, vol. 54, no. 6, pp. 2930–2945, Dec. 2007.
[34] L. Franquelo, J. Rodriguez, J. Leon, S. Kouro, R. Portillo, and M. Prats, "The age of multilevel converters arrives," *IEEE Ind. Electron. Mag.*, vol. 2, no. 2, pp. 28–39, Jun. 2008.
[35] J. Rodriguez *et al.*, "Multilevel converters: An enabling technology for high-power applications," *Proc. IEEE*, vol. 97, no. 11, pp. 1786–1817, Nov. 2009.
[36] S. Kouro *et al.*, "Recent advances and industrial applications of multilevel converters," *IEEE Trans. Ind. Electron.*, vol. 57, no. 8, pp. 2553–2580, Aug. 2010.
[37] S. Debnath, J. Qin, B. Bahrani, M. Saeedifard, and P. Barbosa, "Operation, control, and applications of the modular multilevel converter: A review," *IEEE Trans. Power Electron.*, vol. 30, no. 1, pp. 37–53, Jan. 2015.
[38] A. März, T. Bertelshofer, M. Helsper, and M.-M. Bakran, "Comparison of IGBT and SiC MOSFET in resonant application," in *Proc. 20th Eur. Conf. Power Electron. Appl. (EPE ECCE Eur.)*, Sep. 2018, p. 1.
[39] M. Z. Hossain, N. A. Rahim, and J. A. Selvaraj, "Recent progress and development on power DC-DC converter topology, control, design and applications: A review," *Renew. Sustain. Energy Rev.*, vol. 81, pp. 205–230, Jan. 2018.
[40] L. S. Mendonça, T. C. Naidon, G. G. de Freitas, M. L. D. S. Martins, and F. E. Bisogno, "Energy-based normalization for resonant power converters," *IEEE Trans. Power Electron.*, vol. 33, no. 8, pp. 6526–6536, Aug. 2018.
[41] A. Kirubakaran, S. Jain, and R. K. Nema, "A review on fuel cell technologies and power electronic interface," *Renew. Sustain. Energy Rev.*, vol. 13, no. 9, pp. 2430–2440, Dec. 2009.
[42] A. Safaee, M. Karimi-Ghartemani, P. K. Jain, and A. Bakhshai, "Time-domain analysis of a phase-shift-modulated series resonant converter with an adaptive passive auxiliary circuit," *IEEE Trans. Power Electron.*, vol. 31, no. 11, pp. 7714–7734, Nov. 2016.
[43] C. Yao, X. Ruan, X. Wang, and C. K. Tse, "Isolated buck–boost DC/DC converters suitable for wide input-voltage range," *IEEE Trans. Power Electron.*, vol. 26, no. 9, pp. 2599–2613, Sep. 2011.
[44] J. M. Burkhart, R. Korsunsky, and D. J. Perreault, "Design methodology for a very high frequency resonant boost converter," *IEEE Trans. Power Electron.*, vol. 28, no. 4, pp. 1929–1937, Apr. 2013.
[45] J. Hu, A. D. Sagneri, J. M. Rivas, Y. Han, S. M. Davis, and D. J. Perreault, "High-frequency resonant SEPIC converter with wide input and output voltage ranges," *IEEE Trans. Power Electron.*, vol. 27, no. 1, pp. 189–200, Jan. 2012.
[46] L. Zhu, "A novel soft-commutating isolated boost full-bridge ZVS-PWM DC–DC converter for bidirectional high power applications," *IEEE Trans. Power Electron.*, vol. 21, no. 2, pp. 422–429, Mar. 2006.
[47] Z. Zhang, O. C. Thomsen, and M. A. E. Andersen, "Soft-switched dual-input DC–DC converter combining a boost-half-bridge cell and a voltage-fed full-bridge cell," *IEEE Trans. Power Electron.*, vol. 28, no. 11, pp. 4897–4902, Nov. 2013.
[48] S.-H. Kim, M. Ehsani, and C.-S. Kim, "High-voltage power supply using series-connected full-bridge PWM converter for pulsed power applications," *IEEE Trans. Dielectr. Electr. Insul.*, vol. 22, no. 4, pp. 1937–1944, Aug. 2015.
[49] M. Pahlevani, S. Eren, A. Bakhshai, and P. Jain, "A series–parallel current-driven full-bridge DC/DC converter," *IEEE Trans. Power Electron.*, vol. 31, no. 2, pp. 1275–1293, Feb. 2016.
[50] C. W. Tsang, M. P. Foster, D. A. Stone, and D. T. Gladwin, "Analysis and design of LLC resonant converters with capacitor–diode clamp current limiting," *IEEE Trans. Power Electron.*, vol. 30, no. 3, pp. 1345–1355, Mar. 2015.
[51] F. Zhang, F. Z. Peng, and Z. Qian, "Study of the multilevel converters in DC-DC applications," in *Proc. IEEE 35th Annu. Power Electron. Spec. Conf.*, vol. 2, Jun. 2004, pp. 1702–1706.
[52] Y. Gao, N. Faria, and G. J. Kish, "Dynamic model of an interleaved modular multilevel DC-DC converter for MVDC and HVDC systems," in *Proc. IEEE Electr. Power Energy Conf. (EPEC)*, Oct. 2017, pp. 1–8, doi: 10.1109/EPEC.2017.8286223.
[53] P. Barbosa, P. Steimer, L. Meysenc, M. Winkelnkemper, J. Steinke, and N. Celanovic, "Active neutral-point-clamped multilevel converters," in *Proc. IEEE 36th Conf. Power Electron. Spec. (PESC)*, Jun. 2005, pp. 2296–2301.
[54] A. Coccia, F. Canales, P. Barbosa, and S. Ponnaluri, "Wide input voltage range compensation in DC/DC resonant architectures for on-board traction power supplies," in *Proc. Eur. Conf. Power Electron. Appl.*, 2007, pp. 1–10, doi: 10.1109/EPE.2007.4417709.
[55] F. Liu, G. Hu, and X. Ruan, "Three-phase three-level DC/DC converter for high input voltage and high power applications-adopting symmetrical duty cycle control," *IEEE Trans. Power Electron.*, vol. 29, no. 1, pp. 56–65, Jan. 2014.
[56] K.-M. Yoo and J.-Y. Lee, "A 10-kW two-stage isolated/bidirectional DC/DC converter with hybrid-switching technique," *IEEE Trans. Ind. Electron.*, vol. 60, no. 6, pp. 2205–2213, Jun. 2013.
[57] J. Adhikari, A. K. Rathore, and S. K. Panda, "Modelling, design and control of grid connected converter for high altitude wind power application," in *Proc. Int. Power Electron. Conf. (IPEC-Hiroshima-ECCE ASIA)*, May 2014, pp. 1775–1780.
[58] Z. Pan, F. Zhang, and F. Z. Peng, "Power losses and efficiency analysis of multilevel DC-DC converters," in *Proc. 20th Annu. IEEE Appl. Power Electron. Conf. Expo. (APEC)*, vol. 3, Mar. 2005, pp. 1393–1398.
[59] F. Z. Peng, F. Zhang, and Z. Qian, "A magnetic-less DC-DC converter for dual voltage automotive systems," in *Proc. 37th IAS Annu. Meeting IEEE Ind. Appl. Conf.*, vol. 2, Oct. 2002, pp. 1303–1310.
[60] A. A. A. Hafez, "Multi-level cascaded DC/DC converters for PV applications," *Alexandria Eng. J.*, vol. 54, no. 4, pp. 1135–1146, Dec. 2015.
[61] J. A. Morales-Saldana, E. E. C. Guti, and J. Leyva-Ramos, "Modeling of switch-mode DC-DC cascade converters," *IEEE Trans. Aerosp. Electron. Syst.*, vol. 38, no. 1, pp. 295–299, Jan. 2002.
[62] W. Cai, B. Fahimi, E. Cosoroaba, and F. Yi, "Stability analysis and voltage control method based on virtual resistor and proportional voltage feedback loop for cascaded DC-DC converters," in *Proc. IEEE Energy Convers. Congr. Expo. (ECCE)*, Sep. 2014, pp. 3016–3022.
[63] M. G. Kashani, M. Mobarrez, and S. Bhattacharya, "Variable interleaving technique for photovoltaic cascaded DC-DC converters," in *Proc. 40th Annu. Conf. IEEE Ind. Electron. Soc. (IECON)*, Oct. 2014, pp. 5612–5617.
[64] F. H. Khan and L. M. Tolbert, "A multilevel modular capacitor-clamped DC–DC converter," *IEEE Trans. Ind. Appl.*, vol. 43, no. 6, pp. 1628–1638, Dec. 2007.
[65] T. Jalakas, D. Vinnikov, and J. Laugis, "Development of 50-kW isolated DC/DC converter with high-voltage IGBTs," in *Proc. Compat. Power Electron.*, May 2007, pp. 1–6, doi: 10.1109/CPE.2007.4296566.
[66] O. A. Eno, D. S. Thompson, and J. Coppin, "High power resonant topology for DC-DC converter," in *Proc. Eur. Conf. Power Electron. Appl.*, 2005,

pp. 1–7, doi: 10.1109/EPE.2005.219209.
[67] F. Canales, P. Barbosa, and F. C. Lee, "A wide input voltage and load output variations fixed-frequency ZVS DC/DC LLC resonant converter for high-power applications," in *Proc. 37th IAS Annu. Meeting IEEE Ind. Appl. Conf.*, vol. 4, Oct. 2002, pp. 2306–2313.
[68] J. Jacobs, A. Averberg, and R. De Doncker, "A novel three-phase DC/DC converter for high-power applications," in *Proc. 35th Annu. Power Electron. Spec. Conf. (PESC)*, vol. 3, 2004, pp. 1861–1867.
[69] J. W. Kolar and F. C. Zach, "A novel three-phase utility interface minimizing line current harmonics of high-power telecommunications rectifier modules," *IEEE Trans. Ind. Electron.*, vol. 44, no. 4, pp. 456–467, Aug. 1997.
[70] C. Liu, A. Ridenour, and J.-S. Lai, "Modeling and control of a novel six-leg three-phase high-power converter for low voltage fuel cell applications," *IEEE Trans. Power Electron.*, vol. 21, no. 5, pp. 1292–1300, Sep. 2006.
[71] J.-G. Cho, J.-W. Baek, C.-Y. Jeong, D.-W. Yoo, and K.-Y. Joe, "Novel zero-voltage and zero-current-switching full bridge PWM converter using transformer auxiliary winding," *IEEE Trans. Power Electron.*, vol. 15, no. 2, pp. 250–257, Mar. 2000.
[72] J. Walter and R. W. De Doncker, "High-power galvanically isolated DC/DC converter topology for future automobiles," in *Proc. IEEE 34th Annu. Conf. Power Electron. Specialist. (PESC)*, vol. 1, Jun. 2003, pp. 27–32.
[73] J. Zhang, F. Zhang, X. Xie, D. Jiao, and Z. Qian, "A novel ZVS DC/DC converter for high power applications," *IEEE Trans. Power Electron.*, vol. 19, no. 2, pp. 420–429, Mar. 2004.
[74] A. J. Mason and P. K. Jain, "New ZVS-PSM-FB DC/DC converters with adaptive energy storage for high power SOFC application," in *Proc. 14th IAS Annu. Meeting Conf. Rec. Ind. Appl. Conf.*, vol. 1, 2005, pp. 607–613.
[75] M. Pavlovsky, S. W. H. de Haan, and J. A. Ferreira, "Concept of 50 kW DC/DC converter based on ZVS, quasi-ZCS topology and integrated thermal and electromagnetic design," in *Proc. Eur. Conf. Power Electron. Appl.*, 2005, pp. 1–9, doi: 10.1109/EPE.2005.219307.
[76] C. Liu, A. Johnson, and J.-S. Lai, "A novel three-phase high-power soft-switched DC/DC converter for low-voltage fuel cell applications," *IEEE Trans. Ind. Appl.*, vol. 41, no. 6, pp. 1691–1697, Dec. 2005.
[77] T. Boles, "GaN-on-silicon—Present capabilities and future directions," in *Proc. AIP Conf.*, vol. 1, 2018, pp. 20001–200010.
[78] B. Ozpineci, L. M. Tolbert, S. K. Islam, and M. Hasanuzzaman, "Effects of silicon carbide (SiC) power devices on HEV PWM inverter losses," in *Proc. 27th Annu. Conf. IEEE Ind. Electron. Soc. (IECON)*, vol. 2, Nov. 2001, pp. 1061–1066.
[79] H. Zhang, L. M. Tolbert, and B. Ozpineci, "Impact of SiC devices on hybrid electric and plug-in hybrid electric vehicles," *IEEE Trans. Ind. Appl.*, vol. 47, no. 2, pp. 912–921, Mar. 2011.
[80] L. M. Tolbert, B. Ozpineci, S. K. Islam, and M. S. Chinthavali, "Wide bandgap semiconductors for utility applications," *Semiconductors*, vol. 1, pp. 1–3, Feb. 2005, doi: 10.2172/886008.
[81] H. Jain, S. Rajawat, and P. Agrawal, "Comparision of wide band gap semiconductors for power electronics applications," in *Proc. Int. Conf. Recent Adv. Microw. Theory Appl.*, Nov. 2008, pp. 878–881.
[82] A. P. Zhang *et al.*, "Lateral $Al_xGa_{1-x}N$ power rectifiers with 9.7 kV reverse breakdown voltage," *Appl. Phys. Lett.*, vol. 78, no. 6, pp. 823–825, Feb. 2001.
[83] H. Li, C. Yao, L. Fu, X. Zhang, and J. Wang, "Evaluations and applications of GaN HEMTs for power electronics," in *Proc. IEEE 8th Int. Power Electron. Motion Control Conf. (IPEMC-ECCE Asia)*, May 2016, pp. 563–569.
[84] C. R. Mueller, A. Philippou, C. Jaeger, M. Seifert, A. Vellei, and M. Fugger, "New 1200 V IGBT and diode technology with improved controllability for superior performance in drives application," in *Proc. Int. Exhib. Conf. Power Electron., Intell. Motion, Renew. Energy Energy Manage. (VDE PCIM Eur.)*, 2018, pp. 289–296.
[85] K.-Y. Wong, W. Chen, and K. J. Chen, "Integrated voltage reference generator for GaN smart power chip technology," *IEEE Trans. Electron Devices*, vol. 57, no. 4, pp. 952–955, Apr. 2010.
[86] A. P. Zhan *et al.*, "Comparison of GaN p-i-n and Schottky rectifier performance," *IEEE Trans. Electron Devices*, vol. 48, no. 3, pp. 407–411, Mar. 2001.
[87] T. Boles *et al.*, "High-voltage GaN-on-silicon Schottky diodes," in *Proc. CS MANTECH Conf.*, 2013, pp. 297–300.
[88] M. Asif Khan, J. Kuznia, D. Olson, W. Schaff, J. Burm, and M. Shur, "Microwave performance of a 0.25 μm gate AlGaN/GaN heterostructure field effect transistor," *Appl. Phys. Lett.*, vol. 65, no. 9, pp. 1121–1123, 1994.
[89] Y.-F. Wu, M. Moore, A. Saxler, T. Wisleder, and P. Parikh, "40-W/mm double field-plated GaN HEMTs," in *Proc. 64th Device Res. Conf.*, Jun. 2006, pp. 151–152.
[90] N. Ikeda, S. Kaya, J. Li, Y. Sato, S. Kato, and S. Yoshida, "High power AlGaN/GaN HFET with a high breakdown voltage of over 1.8 kV on 4 inch Si substrates and the suppression of current collapse," in *Proc. 20th Int. Symp. Power Semiconductor Devices IC's*, May 2008, pp. 287–290.
[91] T. Oku, Y. Kamo, and M. Totsuka, "AlGaN/GaN HEMTs passivated by cat-CVD SiN film," *Thin Solid Films*, vol. 516, no. 5, pp. 545–547, Jan. 2008.
[92] S. Yoshida *et al.*, "Fabrication of AlGaN/GaN HFET with a high breakdown voltage of over 1050 V," in *Proc. IEEE Int. Symp. Power Semiconductor Devices ICs*, Jun. 2006, pp. 1–4, doi: 10.1109/ISPSD.2006.1666135.
[93] E. Bahat-Treidel, F. Brunner, O. Hilt, E. Cho, J. Wurfl, and G. Trankle, "AlGaN/GaN/GaN:C back-barrier HFETs with breakdown voltage of over 1 kV and low $R_{ON} \times A$," *IEEE Trans. Electron Devices*, vol. 57, no. 11, pp. 3050–3058, Sep. 2010.
[94] P. Srivastava *et al.*, "Record breakdown voltage (2200 V) of GaN DHFETs on Si with 2-μm buffer thickness by local substrate removal," *IEEE Electron Device Lett.*, vol. 32, no. 1, pp. 30–32, Dec. 2011.
[95] K. S. Boutros, S. Chandrasekaran, W. B. Luo, and V. Mehrotra, "GaN switching devices for high-frequency, KW power conversion," in *Proc. IEEE Int. Symp. Power Semiconductor Devices ICs*, Jun. 2006, pp. 1–4, doi: 10.1109/ISPSD.2006.1666136.
[96] W. Saito, Y. Takada, M. Kuraguchi, K. Tsuda, and I. Omura, "Recessed-gate structure approach toward normally off high-voltage AlGaN/GaN HEMT for power electronics applications," *IEEE Trans. Electron Devices*, vol. 53, no. 2, pp. 356–362, Feb. 2006.
[97] Y. Cai, Y. Zhou, K. M. Lau, and K. J. Chen, "Control of threshold voltage of AlGaN/GaN HEMTs by fluoride-based plasma treatment: From depletion mode to enhancement mode," *IEEE Trans. Electron Devices*, vol. 53, no. 9, pp. 2207–2215, Sep. 2006.
[98] T. Palacios, C.-S. Suh, A. Chakraborty, S. Keller, S. P. DenBaars, and U. K. Mishra, "High-performance E-mode AlGaN/GaN HEMTs," *IEEE Electron Device Lett.*, vol. 27, no. 6, pp. 428–430, Jun. 2006.
[99] X. Hu, G. Simin, J. Yang, M. A. Khan, R. Gaska, and M. S. Shur, "Enhancement mode AlGaN/GaN HFET with selectively grown pn junction gate," *Electron. Lett.*, vol. 36, no. 8, pp. 753–754, Apr. 2000.
[100] W. Huang, Z. Li, T. Chow, Y. Niiyama, T. Nomura, and S. Yoshida, "Enhancement-mode GaN hybrid MOS-HEMTs with $R_{on,sp}$ of 20 mω-cm^2," in *Proc. 20th Int. Symp. Power Semiconductor Devices IC's*, 2008, pp. 295–298.
[101] R. Mitova, R. Ghosh, U. Mhaskar, D. Klikic, M.-X. Wang, and A. Dentella, "Investigations of 600-V GaN HEMT and GaN diode for power converter applications," *IEEE Trans. Power Electron.*, vol. 29, no. 5, pp. 2441–2452, May 2014.
[102] B. M. Green *et al.*, "Cascode connected AlGaN/GaN HEMTs on SiC substrates," *IEEE Microw. Guided Wave Lett.*, vol. 10, no. 8, pp. 316–318, Aug. 2000.
[103] F. Roccaforte, G. Greco, P. Fiorenza, and F. Iucolano, "An overview of normally-off GaN-based high electron mobility transistors," *Materials*, vol. 12, no. 10, p. 1599, May 2019, doi: 10.3390/ma12101599.
[104] R. Ramachandran and M. Nymand, "Experimental demonstration of a 98.8% efficient isolated DC–DC GaN converter," *IEEE Trans. Ind. Electron.*, vol. 64, no. 11, pp. 9104–9113, Nov. 2017.
[105] A. M. Elrajoubi, K. George, and S. S. Ang, "Investigation of a new GaN AC/DC topology for battery charging application," in *Proc. IEEE Texas Power Energy Conf. (TPEC)*, Feb. 2018, pp. 1–6, doi: 10.1109/tpec.2018.8312047.
[106] J. Kim and C. Kim, "A DC–DC boost converter with variation-tolerant MPPT technique and efficient ZCS circuit for thermoelectric energy harvesting applications," *IEEE Trans. Power Electron.*, vol. 28, no. 8, pp. 3827–3833, Aug. 2013.
[107] Y. Gu and D. Zhang, "Interleaved boost converter with ripple cancellation network," *IEEE Trans. Power Electron.*, vol. 28, no. 8, pp. 3860–3869, Aug. 2013.
[108] C.-L. Wei, C.-H. Chen, K.-C. Wu, and I.-T. Ko, "Design of an average-current-mode noninverting buck–boost DC–DC converter with reduced switching and conduction losses," *IEEE Trans. Power Electron.*, vol. 27, no. 12, pp. 4934–4943, Dec. 2012.
[109] J. Marcos Alonso, D. Gacio, F. Sichirollo, Á. R. Seidel, and M. A. Dalla Costa, "A straightforward methodology to modeling high power factor AC–DC converters," *IEEE Trans. Power Electron.*, vol. 28, no. 10, pp. 4723–4731, Oct. 2013.
[110] S. U. Hasan and G. E. Town, "An aperiodic modulation method to mitigate electromagnetic interference in impedance source DC–DC converters," *IEEE Trans. Power Electron.*, vol. 33, no. 9, pp. 7601–7608, Sep. 2018.
[111] J. A. Martinez-Velasco and J. Martin-Arnedo, "Power electronics applications," in *Transient Analysis of Power Systems: A Practical Approach*. Hoboken, NJ, USA: Wiley, 2020, ch. 8, pp. 333–404.
[112] A. Alzahrani, M. Ferdowsi, and P. Shamsi, "A family of scalable non-isolated interleaved DC-DC boost converters with voltage multiplier cells," *IEEE Access*, vol. 7, pp. 11707–11721, 2019.
[113] Y. K. Ramadass and A. P. Chandrakasan, "Voltage scalable switched capacitor DC-DC converter for ultra-low-power on-chip applications," in *Proc. IEEE Power Electron. Specialists Conf.*, Jun. 2007, pp. 2353–2359.
[114] Z. Rehman, I. Al-Bahadly, and S. Mukhopadhyay, "Multiinput DC–DC converters in renewable energy applications—An overview," *Renew. Sustain. Energy Rev.*, vol. 41, pp. 521–539, Jan. 2015.
[115] N. A. Khan. *Power Loss Modeling of Isolated AC/DC Converter*. Accessed: 2012. [Online]. Available: http://www.diva-portal.org/smash/get/diva2:583637/FULLTEXT01.pdf
[116] M. A. Rehman-Shaikh, P. D. Mitcheson, and T. C. Green, "Power loss minimization in cascaded multi-level converters for distribution networks," in *Proc. 33rd Annu. Conf. IEEE Ind. Electron. Soc. (IECON)*, Nov. 2007, pp. 1774–1779.
[117] G. Zulauf, S. Park, W. Liang, K. Surakitbovorn, and J. Rivas-Davila, "C_{OSS} losses in 600V GaN power semiconductors in soft-switched, high- and very-high-frequency power converters," *IEEE Trans. Power Electron.*, vol. 33, no. 12, pp. 10748–10763, Dec. 2018.
[118] T. Mishima and E. Morita, "High-frequency bridgeless rectifier based ZVS multiresonant

converter for inductive power transfer featuring high-voltage GaN-HFET," *IEEE Trans. Ind. Electron.*, vol. 64, no. 11, pp. 9155–9164, Nov. 2017.

[119] P. Niknejad, T. Agarwal, and M. R. Barzegaran, "Using gallium nitride DC-DC converter for speed control of BLDC motor," in *Proc. IEEE Int. Electric Mach. Drives Conf. (IEMDC)*, May 2017, pp. 1–6, doi: 10.1109/IEMDC.2017.8002237.

[120] A. M. S. Al-bayati, S. S. Alharbi, S. S. Alharbi, and M. Matin, "A comparative design and performance study of a non-isolated DC-DC buck converter based on Si-MOSFET/Si-diode, SiC-JFET/SiC-Schottky diode, and GaN-transistor/SiC-Schottky diode power devices," in *Proc. North Amer. Power Symp. (NAPS)*, Sep. 2017, pp. 1–6, doi: 10.1109/naps.2017.8107192.

[121] A. M. S. Al-bayati and M. Matin, "A highly efficient GaN E–HEMT/SiC Schottky diode power device based DC–DC ZETA converter," in *Proc. IEEE Conf. Technol. Sustainability (SusTech)*, Nov. 2018, pp. 1–5, doi: 10.1109/sustech.2018.8671330.

[122] S. S. Alharbi, S. S. Alharbi, and M. Matin, "An improved interleaved DC-DC SEPIC converter based on SiC-cascade power devices for renewable energy applications," in *Proc. IEEE Int. Conf. Electro/Inf. Technol. (EIT)*, May 2018, pp. 0487–0492.

[123] X. Wang, L. Zhang, B. Wang, Z. Yang, Y. Fu, and K. Zha, "Design of bidirectional isolated DC/DC converter based on SiC device," in *Proc. IEEE 10th Int. Symp. Power Electron. Distrib. Gener. Syst. (PEDG)*, Jun. 2019, pp. 688–692.

[124] M. Kanamura *et al.*, "Enhancement-mode GaN MIS-HEMTs with n-GaN/i-AlN/n-GaN triple cap layer and high-k gate dielectrics," *IEEE Electron Device Lett.*, vol. 31, no. 3, pp. 189–191, Feb. 2010.

[125] W.-S. Choi and S.-M. Young, "Effectiveness of a SiC Schottky diode for super-junction MOSFETs on continuous conduction mode PFC," in *Proc. SPEEDAM*, Jun. 2010, pp. 562–567.

[126] S. Park and J. Rivas-Davila, "Power loss of GaN transistor reverse diodes in a high frequency high voltage resonant rectifier," in *Proc. IEEE Appl. Power Electron. Conf. Expo. (APEC)*, Mar. 2017, pp. 1942–1945.

[127] M. Moradpour and G. Gatto, "A new SiC-GaN-based two-phase interleaved bidirectional DC-DC converter for plug-in electric vehicles," in *Proc. Int. Symp. Power Electron., Electr. Drives, Autom. Motion (SPEEDAM)*, Jun. 2018, pp. 587–592.

[128] C. Qian *et al.*, "Thermal management on IGBT power electronic devices and modules," *IEEE Access*, vol. 6, pp. 12868–12884, 2018.

[129] X. Guo, Q. Xun, Z. Li, and S. Du, "Silicon carbide converters and MEMS devices for high-temperature power electronics: A critical review," *Micromachines*, vol. 10, no. 6, p. 406, Jun. 2019.

ABOUT THE AUTHORS

Mohammad Parvez received the B.Sc. degree in electrical and electronic engineering from the Dhaka University of Engineering and Technology (DUET), Gazipur, Bangladesh, in 2010, and the M.Phil. degree in power electronics and control from the University of Malaya, Kuala Lumpur, Malaysia, in 2017. He is currently working toward the Ph.D. degree at the School of Electrical and Electronic Engineering, The University of Adelaide, Adelaide, SA, Australia.

From 2011 to 2013, he worked at a 50-MW peaking power plant in Comilla, Bangladesh, as an Assistant Engineer (operation & maintenance). His research interests include grid-connected PV inverters, power electronics, and renewable energy.

Aaron T. Pereira (Member, IEEE) received the B.E. degree in microelectronic engineering from Griffith University, Nathan, QLD, Australia, in 2004, the master's degree in project management (MPM) from The University of Adelaide, Adelaide, SA, Australia, in 2009, the M.E. degree in wireless engineering from The University of Sydney, Sydney, NSW, Australia, in 2010, and the Ph.D. degree in electronic engineering from Macquarie University, Sydney, in 2016.

From 2004 to 2009, he worked in various roles as an RF design engineer, a systems engineer, and project management positions at the Australian Space and Defence Industry. From 2011 to 2012, he was a Visiting Scholar with the University of Colorado Boulder, Boulder, CO, USA. From 2012 to 2013, he was a Visiting Scientist with the Fraunhofer Institute for Applied Solid State Physics (IAF), Freiburg im Breisgau, Germany. In 2016, he embarked on a postdoctoral research program at the School of Electrical and Electronic Engineering, The University of Adelaide. As a Sir Keith Murdoch Fellow, he is currently collaborating at the Jet Propulsion Laboratory, NASA/Caltech, Pasadena, CA, USA. His research interests include gallium–nitride (GaN) power chips, trap characterization, switch models, and mm-wave GaN power amplifiers (PAs) for aerospace applications.

Dr. Pereira was awarded an Endeavor Australia Executive Fellowship in 2018, which allowed him to visit JPL and to gain a holistic understanding of various systems involved in interplanetary missions, including imaging sensors and radars. He then also won the South Australian Space Industry Fund Scholarship and the Sir Keith Murdoch Postdoctoral Fellowship awarded by the America Australia Association (AAA) in 2019.

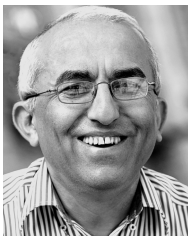

Nesimi Ertugrul (Senior Member, IEEE) received the B.Sc. degree in electrical engineering and the M.Sc. degree in electronic and communication engineering from Istanbul Technical University, Istanbul, Turkey, in 1985 and 1989, respectively, and the Ph.D. degree in electrical and electronic engineering from the University of Newcastle, Newcastle upon Tyne, U.K., in 1993.

Since 1994, he has been with The University of Adelaide, Adelaide, SA, Australia, where he is currently an Associate Professor. He is the author of the book *LabVIEW for Electric Circuits, Machines, Drives, and Laboratories* (Prentice-Hall, 2002). His primary research interests include sensorless operation of switched machines, power electronics, renewable energy systems, fault-tolerant motor drives, power quality monitoring, condition monitoring, and battery storage systems.

Neil H. E. Weste (Life Fellow, IEEE) received the B.Sc., B.E. (Elec.), and Ph.D. degrees in electrical engineering from the University of Adelaide, Adelaide, SA, Australia, in 1973, 1974, and 1978, respectively.

In 1977, he commenced working at Bell Labs, Holmdel, NJ, USA, in the area of IC design. Subsequently, he spent a year in North Carolina, USA, primarily at Duke University, Durham, NC, USA, the University of North Carolina at Chapel Hill (Chapel Hill), Chapel Hill, NC, USA, and MCNC, Research Triangle, NC, USA, building VLSI design capabilities in that state. After returning to Bell Labs for a year, he joined Symbolics Inc., Cambridge, MA, working on single-chip Lisp computers (Ivory). He cofounded TLW Inc., Burlington, MA, where he designed many custom ICs for a variety of companies. In 1995, he joined Macquarie University, Sydney, NSW, Australia. In 1997, he cofounded Radiata Communications, Sydney, NSW, working on WLAN chips. He later worked at Cisco Systems, Sydney, NSW, after the acquisition of Radiata Communications in 2000. He then became an angel investor, and after developing an interest in flying, he cofounded OzRunways Pty., Ltd., Mawson Lakes, SA, Australia, where he cowrote the software that is now used by the majority of pilots in Australia in their Electronic Flight Books. He is currently an Adjunct Professor with the School of Electrical and Electronic Engineering, The University of Adelaide.

Dr. Weste is a Fellow of the Australian Academy of Technology and Engineering (ATSE). He was awarded the D.E. (honoris causa) from The University of Adelaide in 2004 and received the 2010 Clunies Ross Medal for his contributions to the development of Wi-Fi.

Derek Abbott (Fellow, IEEE) was born in London, U.K. He received the B.Sc. degree (honors) in physics from Loughborough University, Loughborough, U.K., in 1982, and the Ph.D. degree in electrical and electronic engineering from The University of Adelaide, Adelaide, SA, Australia, in 1995, under K. Eshraghian and B. R. Davis.

From 1978 to 1986, he was a Research Engineer with the GEC Hirst Research Centre, London. From 1986 to 1987, he was a VLSI Design Engineer with Austek Microsystems, Adelaide, SA. Since 1987, he has been with The University of Adelaide, where he is currently a Full Professor with the School of Electrical and Electronic Engineering. He coedited the book *Quantum Aspects of Life* (London, U.K.: Imperial College Press, 2008) and coauthored *Stochastic Resonance* (Cambridge, U.K.: Cambridge University Press, 2012) and *Terahertz Imaging for Biomedical Applications* (New York, NY, USA: Springer-Verlag, 2012). His interests are in the areas of multidisciplinary physics and electronic engineering applied to complex systems. His research programs span a number of areas of stochastics, game theory, photonics, renewable energy, energy policy, biomedical engineering, and computational neuroscience.

Prof. Abbott is a Fellow of the Institute of Physics (IoP), U.K., and an Honorary Fellow of Engineers Australia. He has won a number of awards, including the South Australian Tall Poppy Award for Science in 2004, the Premier's SA Great Award in Science and Technology for outstanding contributions to South Australia in 2004, the Australian Research Council Future Fellowship in 2012, the David Dewhurst Medal in 2015, the Barry Inglis Medal in 2018, and the M. A. Sargent Medal in 2019 for eminence in engineering. He has served as an Editor and/or Guest Editor for a number of journals, including the IEEE JOURNAL OF SOLID-STATE CIRCUITS, the *Journal of Optics B*, the *Microelectronics Journal*, *Chaos*, *Smart Structures and Materials, Fluctuation and Noise Letters*, the PROCEEDINGS OF THE IEEE, and the IEEE PHOTONICS JOURNAL. He is also on the editorial boards of IEEE ACCESS, *Frontiers in Physics*, *Royal Society Open Science*, and *Scientific Reports* (Nature). He is also the Editor-in-Chief (EIC) of IEEE ACCESS and serves on the IEEE Publication Services and Products Board (PSPB).

Said F. Al-Sarawi (Member, IEEE) received the General Certificate in marine radio communication and the B.Eng. degree (honors) in marine electronics and communication from the Arab Academy for Science and Technology, Alexandria, Egypt, in 1987 and 1990, respectively, and the Ph.D. degree in mixed analog and digital circuit design techniques for smart wireless systems with special commendation in electrical and electronic engineering and the Graduate Certificate in education (higher education) from The University of Adelaide, Adelaide, SA, Australia, in 2003 and 2006, respectively.

He is currently the Director of the Centre for Biomedical Engineering and a Founding Member of the Education Research Group of Adelaide, The University of Adelaide. His research interests include design techniques for mixed-signal systems in complementary metal–oxide–semiconductor and optoelectronic technologies for high-performance radio transceivers, low-power and low-voltage radio frequency identification systems, data converters, mixed-signal design, and microelectromechanical systems for biomedical applications. His current educational research is focused on innovative teaching techniques for engineering education, research skill development, and factors affecting student's evaluations of courses in different disciplines.

Dr. Al-Sarawi received The University of Adelaide Alumni Postgraduate Medal (formerly Culross Prize) for outstanding academic merit at the postgraduate level. While pursuing the Ph.D. degree, he won the Commonwealth Postgraduate Research Award (Industry).